CB-Note 307

Decay distributions of $\eta' \to \pi^+\pi^-\gamma$ and $\eta \to \pi^+\pi^-\pi^0$ Technical Report

Fritz-Herbert Heinsius
University of California, Berkeley
and
Maurice Benayoun
LPNHE des Universités Paris VI et VII,IN2P3–CNRS, F–75252 Paris, France

November 12, 1996

Abstract

The distribution of $m(\pi^+\pi^-)$ in the decay $\eta' \to \pi^+\pi^-\gamma$ has been measured. The η' has been produced in the reactions $p\bar{p} \to \pi^0\pi^0\eta'$, $p\bar{p} \to \pi^+\pi^-\eta'$ and $p\bar{p} \to \omega\eta'$. The results are based on a total of 6910 η' decays extracted from 10 million 2-prong and 2 million 4-prong triggered data.

In a further study the box anomaly constant is extracted from this spectrum and the pseudoscalar parameters (f_1, f_8 and θ_{PS}) are determined.

In a second analysis the distribution of the π^0 momentum of the $\eta \to \pi^+\pi^-\pi^0$ decay is measured. This is based on 3329 events of the type $\overline{p}p \to \pi^0\pi^0\eta$, $\eta \to \pi^+\pi^-\pi^0$.

Details of the analyses are described in this note.

1 Introduction

This CB-note describes two different analyses. Because both are based on the same data sample and the same selection methods they are presented together. After the general data selection in section 2 the cuts for the event selection are listed in section 3. Section 4 describes the analysis of the decay distribution of $\eta' \to \pi^+\pi^-\gamma$. This process is relevant in order to check whether the box anomaly predicted by current algebra and chiral theories exists and can be extracted from our data; moreover this will allow us to work out the test of QCD formerly proposed by Chanowitz [1, 2], which relies on the knowledge of the box and triangle anomalies for the η and η' mesons. Details about the physics motivation can be found in [3, 4]. The determination of the box anomaly constant and the pseudoscalar parameters (f_1, f_8 and θ_{PS}) are described in section 5. In section 6 the Dalitz plot $\eta \to \pi^+\pi^-\pi^0$ is analyzed. The results from the Crystal Barrel paper [5] are improved to allow better tests of the theoretical predictions by the chiral perturbation theory [6].

2 Data selection and production

This analysis is based on 10.7 million 2-prong events taken in June 1994 and 1.6 million 4-prong events taken in June 1991. The selected tapes have gone through run by run quality checks done by the CERN group. Additionally variations against run number of basic event parameters such as average particle multiplicities and energies were checked. The Menu program input files for these checks can be found in ``http://nsdssp.lbl.gov/cb/quality''.

In the beginning of the June 1994 data taking period the 2-prong trigger was changed from JDC layer 20 and 21 to layer 19 and 20 due to a trigger inefficiency in one sector of layer 21. Therefore only runs 22570 to 23334 were analyzed. Runs 22696, 22701 and 22702 were excluded because of a malfunction of a MALU unit in the PWC trigger.

From the June 91 4-prong run period tapes GD0824 to GD0852 are used and the following runs are excluded from analysis: 6863 - 6901 (number of tracks too high, runbook says FERA errors), 7197 - 7243 (number of tracks too high) and 7432 - 7437 (number of tracks too low, runbook says new JDC readout tests).

All datasets were reproduced using the FFUZ pattern recognition and the newest offline software (see Table 1 and 2).

	June 91		June 94		Monte Carlo	
program	version	date	version	date	version	date
CBOFF	1.28/04	22/06/95	1.30/04	15/04/96	1.30/04	15/04/96
BCTRAK	2.03/00	07/04/95	2.04/01	14/02/96	2.04/01	14/02/96
LOCATER	1.99/14	13/07/95	2.01/05	02/04/96	2.01/08	27/06/96
GTRACK	1.34/01	18/04/95	1.36/01	14/02/96	1.36/01	14/02/96
CCDBCB	2.04/02	23/06/95	2.05/00	24/08/95	2.05/00	24/08/95
CBDROP	1.11/01	16/12/95	1.11/01	16/12/95	1.11/01	16/12/95
CBKFIT	3.09/00	25/07/95	3.09/00	25/07/95	3.09/00	25/07/95

Table 1: Program versions used for reconstruction and analysis.

Monte Carlo datasets were generated using CBGEANT version 5.05/01 and 5.05/03 linked with Geant 3.21/05. This data was run through the same analysis chain as the data.

constants	June 91 date	June 94 date	Monte Carlo new (old) JDC date
alignment JDC-barrel	940714	940920	920227
bad run list	920205	940921	
B field	920205	940920	-15
air pressure	940712	950403	725
Barrel lookup table	920214	on tape	on tape
FERA/2282 pedestals	on tape	on tape	on tape
FERA ped correction	911114	on tape	on tape
Energy calibration	911220	940926	920309
FERA/2282 ratios	911114	940814	920127
bad crystal info	all crystals ok	951103	all crystals set ok
PED spline parameter	921117	921117	921117
JDC z calibration	940712	950406	920127
JDC time to distance	940325	941202	941202 (940325)
wire dE/dx constants	951603	950620	920312
bad wire info	920206	950324	920127
JDC card file	940712	950405	950105
dE/dx polynom coef	951603	950620	920312
JDC +z -Z Endplate	940712	950406	940324
fudge coefficients	940706	none	none

Table 2: Calibration dates.

Sample Monte Carlo input file for the old JDC:

```
LIST
* give run number and number of first event
RUNG    109     1
* random generator seed1,seed2
RNDM    109     0
* number of events
TRIG    60000
* print event x to y
DEBUG 1 10
* chose what to print
PRINT   'VERT' 'KINE'
* JDC version 1 or 2
JDCD 1
* assign configfile for the JDC gas
JDC      'jdc1_15.dat'
* assign configfile FERA lookuptable
LUTF      'mcfera.lut'
* assign configfile 2282 lookuptable
LUT2      'mc2282.lut'
*     3  hit/mc pz   nrpar   part_ids
KINE  3  1.0    0.0 2.0 65. 81.
```

```
* list of data to be written
*   output unit
RAWD  20       'EVHD' 'RPWC' 'RJDC' 'RBCL' 'RBCF' 'RMCB'
*   stop 180 seconds before end of cpu time, 0.=no limit
TIME      2=180. 3=0.
* set vert of annihilation
SETV 91 0.0 0.0 0.0
* vertex smearing x,y,z
BWID  0.25 0.25 0.2
END
```

and the lines modified for the new JDC:

```
* JDC version 1 or 2
JDCD 2
* assign configfile for the JDC gas
JDC      'jdc2_15.dat'
```

A list of all Monte Carlo datasets can be found in table 3.

Reaction	decay chain		prongs	events
$\overline{p}p \to \omega\eta'$	$\omega \to \pi^0\gamma$	$\eta' \to \pi^+\pi^-\gamma$	2	120 000
$\overline{p}p \to \omega\eta'$	$\omega \to \pi^+\pi^-\pi^0$	$\eta' \to \pi^+\pi^-\gamma$	4	120 000
$\overline{p}p \to \pi^0\pi^0\eta'$		$\eta' \to \pi^+\pi^-\gamma$	2	300 000
$\overline{p}p \to \pi^+\pi^-\eta'$		$\eta' \to \pi^+\pi^-\gamma$	4	110 000
$\overline{p}p \to \pi^0\pi^0\eta$		$\eta \to \pi^+\pi^-\pi^0$	2	140 000

Table 3: Produced Monte Carlo datasets.

3 Event selection

3.1 Optimization of the selection criteria

Cuts for the event selection were studied on a subsample of the data in the prominent signal of $\overline{p}p \to \omega\omega$ where one ω decays into $\pi^0\gamma$ and the other into $\pi^+\pi^-\pi^0$. The objective of this study was to compare the dependence of various cuts on the signal size in data and Monte Carlo simulation. Basic requirements for the selected events were: Exactly two tracks with total charge zero, first hit in layer 3 or less, last hit in layer 19 or further, helix error code 0 or 1 and originating from a common vertex. No Peds in type 13 crystals were allowed. Peds from "charged clusters" were ignored.

The table 4 shows the default cuts. Each cut was modified to the values specified in this table, while leaving all other cuts at their default value. Events surviving these cuts were submitted to the kinematic fit for the 6C hypothesis $\overline{p}p \to \pi^+\pi^-\pi^0\pi^0\gamma$. The effects on the variation in these cuts can be found in table 5 and 6.

Note that this study was performed with a small subsample of the total datasample and therefore the statistical errors are big (around 5%). PED energy cuts are required to minimize uncertainties in the low energy behavior of the Monte Carlo simulation, especially from splitoffs.

	Cut on	default	varied to
1	PED E center crystal >	13	4
2	PED energy >	20	10
3	PED E1/E9 <	no cut	0.96
4	DOLBY-C splitoff	yes	no
5	use CBDROP	yes	no
6	TAXI splitoff	no	yes
7	Last hit >= layer	21	19
8	vertex $-2 < z < 2$	no cut	use cut
9	Track χ^2 <	1.5	no cut
10	Track χ^2 <	1.5	1.6
11	Track χ^2 <	1.5	1.4
12	Track χ^2 <	1.5	1.2

Table 4: List of cuts which were varied.

	Cut	data	variation	MC	variation	data/MC
	Default cuts	872.00	0.00	711.00	0.00	0.00
1	PED center >4	862.00	-0.01	693.00	-0.03	0.01
2	PED energy >10	881.00	0.01	700.00	-0.02	0.03
3	E1/E9 <0.96	836.00	-0.04	670.00	-0.06	0.02
4	disable DOLBY-C	845.00	-0.03	687.00	-0.03	0.00
5	no CBDROP	826.00	-0.05	688.00	-0.03	-0.02
6	enable TAXI	781.00	-0.10	643.00	-0.10	-0.01
7	Layer >=19	909.00	0.04	774.00	0.09	-0.04
8	$-2 < z < 2$ vertex	872.00	0.00	710.00	-0.00	0.00
9	no χ^2 cut	874.00	0.00	712.00	0.00	0.00
10	$\chi^2 < 1.6$	871.00	-0.00	711.00	0.00	-0.00
11	$\chi^2 < 1.4$	864.00	-0.01	703.00	-0.01	0.00
12	$\chi^2 < 1.2$	823.00	-0.06	661.00	-0.07	0.02

Table 5: Fitted $\omega \to \pi^0\gamma$ events after kinematic fit.

Both the DOLBY-C and CBDROP routines were used to efficiently suppress splitoffs. It was found that both the TAXI cuts and the E1/E9 cut reduce the signal and the background by the same amount. Therefore they were not used for the final selection. The χ^2 cut was set to 1.5.

3.2 Cuts

The same set of cuts are used for the 2-prong and 4-prong analysis. These cuts are based on recommendations brought together by the CERN analysis group and the optimizations described in section 3.1.

PED cuts:

- PED central crystal energy > 13 MeV.

	Cut	data	variation	MC	variation	data/MC
	Default cuts	439.00	0.00	684.00	0.00	0.00
1	PED center >4	435.00	-0.01	674.00	-0.01	0.01
2	PED energy >10	432.00	-0.02	673.00	-0.02	0.00
3	E1/E9 <0.96	434.00	-0.01	648.00	-0.05	0.04
4	disable DOLBY-C	453.00	0.03	663.00	-0.03	0.06
5	no CBDROP	435.00	-0.01	671.00	-0.02	0.01
6	enable TAXI	391.00	-0.11	624.00	-0.09	-0.02
7	Layer >=19	446.00	0.02	749.00	0.10	-0.07
8	$-2 < z < 2$ vertex	439.00	0.00	682.00	-0.00	0.00
9	no χ^2 cut	445.00	0.01	688.00	0.01	0.01
10	$\chi^2 < 1.6$	442.00	0.01	685.00	0.00	0.01
11	$\chi^2 < 1.4$	432.00	-0.02	679.00	-0.01	-0.01
12	$\chi^2 < 1.2$	412.00	-0.06	640.00	-0.06	0.00

Table 6: Fitted $\omega \to \pi^+\pi^-\pi^0$ events after kinematic fit.

- PED energy > 20 MeV.
- Not in same cluster as one PED correlated to a track.
- Cos $\alpha < 0.98$ with α angle to nearest track.
- Not a splitoff according to DOLBY-C (default cuts)
- Drop PEDs according to CBDROP information.

Event cuts:

- All PEDs within $21° < \phi < 159°$
- Exactly 2 or 4 tracks
- Sum of charge zero.
- All tracks start before layer 4 and end after layer 20.
- All tracks have no helix error (error code=0 or 1).
- All tracks have $\chi^2 < 1.5$
- All tracks originate from common vertex.
- No pileup flag set.
- Confidence level from kinematic fit above 10%.

3.3 Kinematic fitter

Optimizations for the kinematic fitter were done in two steps. First the energy of the PEDs and the momenta of charged tracks were corrected, the errors were scaled to get the expected pull distributions and a flat confidence level distribution. There are different sets of correction for the June 91 run, which used the old JDC and the June 94 run, the first run with the new JDC. The corrections vary slightly for Monte Carlo data.

Cut	min. bias	2-prong	Monte Carlo
No pileup	0.89	0.86	1.00
No type 13 Peds	0.78	0.85	0.75
2 tracks	0.31	0.91	0.74
Sum charge = 0	0.91	0.97	0.93
First hit < layer 4	0.94	0.95	0.94
Last hit > layer 20	0.56	0.94	0.58
No helix error	0.99	1.00	0.99
Track $chi^2 < 1.5$	0.95	0.95	0.97
Tracks from vertex	1.00	1.00	1.00
More than 1 photon	0.93	0.93	1.00
All cuts:	0.09	0.50	0.27

Table 7: Effects of the cuts on the 2-prong data.

Events were selected with the same selection criteria as used for the final analysis, except that CBDROP was not used, because it is based on a 4C-fit and would have caused an uncorrectable bias. Channels with a different number of photons were selected to make it possible to apply these corrections to a wider range of reactions. In these optimizations the following channels were subjected to kinematic fits:

- $\overline{p}p \rightarrow \pi^+\pi^-\gamma\gamma$ (4C fit)
- $\overline{p}p \rightarrow \pi^+\pi^-3\pi^0$ (7C fit)
- $\overline{p}p \rightarrow 2\pi^+2\pi^-\pi^0$ (5C fit)
- $\overline{p}p \rightarrow 2\pi^+2\pi^-2\pi^0$ (6C fit)

	new JDC		old JDC	
Variable	2-prong data	Monte Carlo	4-prong data	Monte Carlo
$\sqrt{E}$	1.0	1.0	1.0	1.0
z-vertex offset (θ)	0.2	0	0	0
ϕ offset	0.007	0	0	0
p^+_{xy}	1.002	1.004	1.0	1.0
p^-_{xy}	1.006	1.005	1.0	1.0
$1/p^+_{xy}$ offset 0.001/x	0	0	-30	-40
$1/p^-_{xy}$ offset 0.001/x	0	0	-30	-60
tan λ^+ offset	-0.0032	0	0	0
tan λ^- offset	-0.0032	0	0	0
ψ^+ offset	0	0	0	0
ψ^- offset	0	0	0	0

Table 8: Scaling of the 4-vectors.

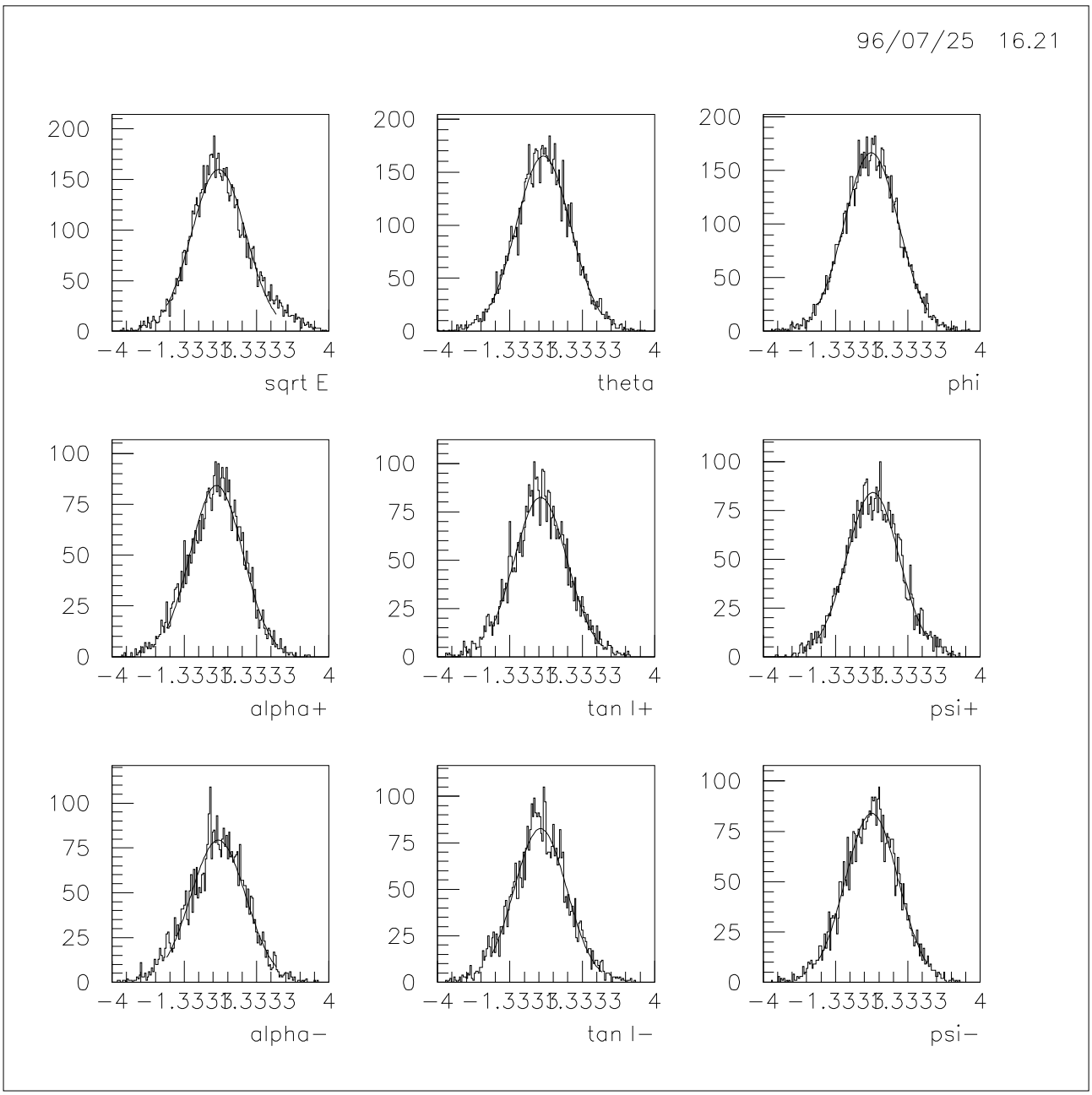

Figure 1: Distribution of pulls for events of the type $\overline{p}p \rightarrow 2\pi^+2\pi^-2\pi^0$. 6C fit with 1% confidence level cut.

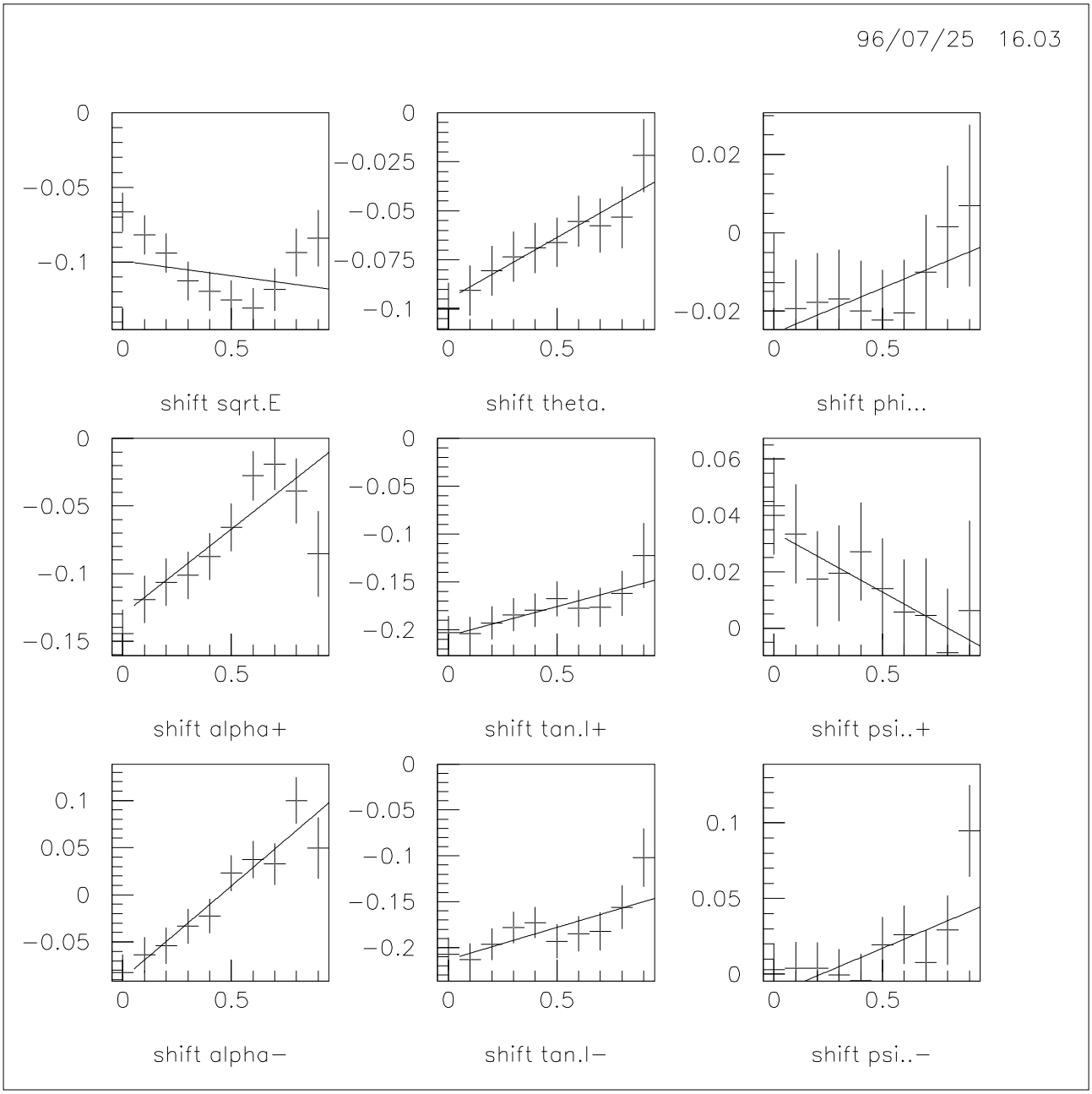

Figure 2: Distribution of shift of pulls for events of the type $\overline{p}p \rightarrow 2\pi^+2\pi^-2\pi^0$ versus the confidence level of the 6C fit.

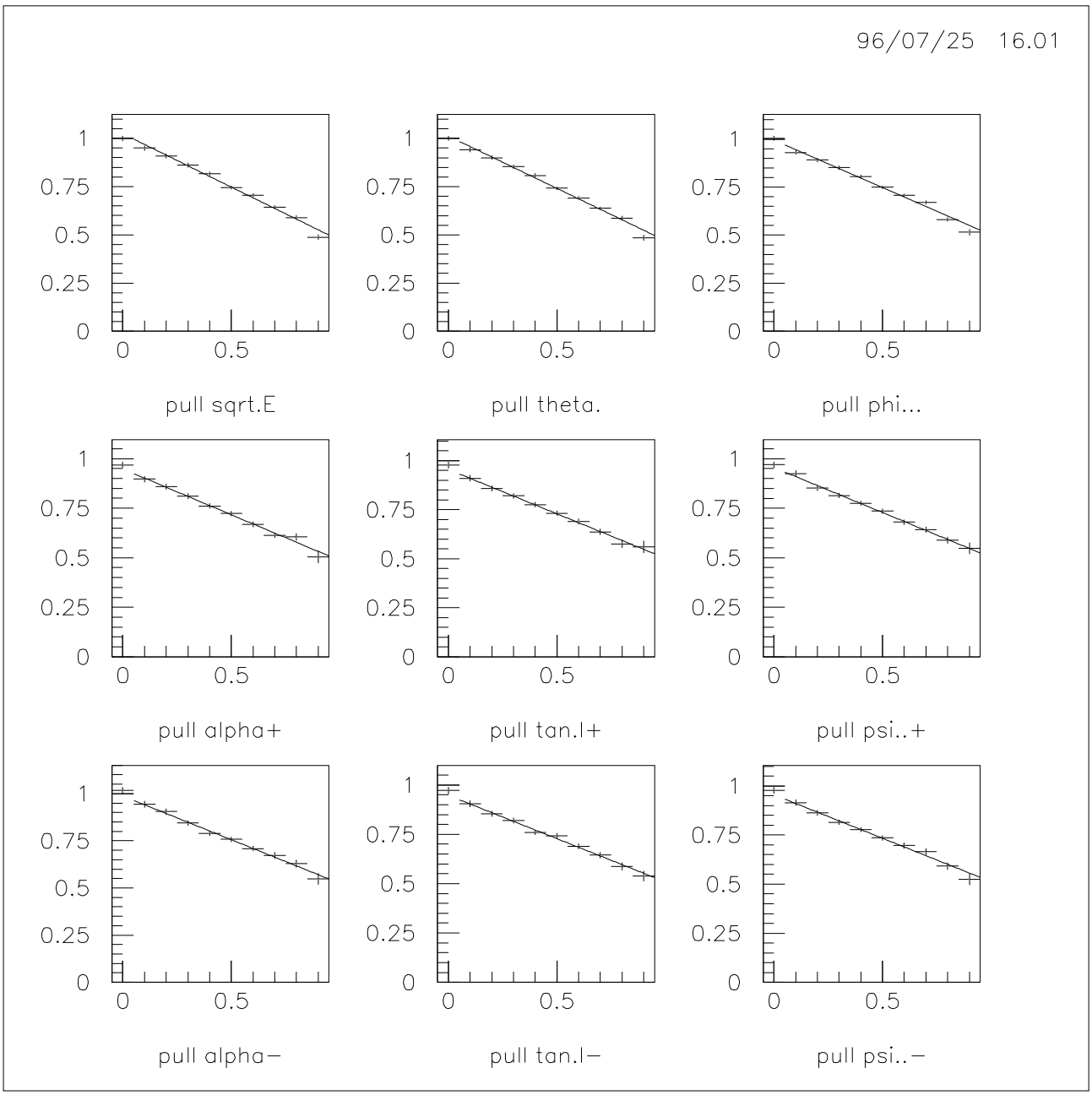

Figure 3: Distribution of sigma of pulls for events of the type $\overline{p}p \to 2\pi^+2\pi^-2\pi^0$ versus the confidence level of the 6C fit.

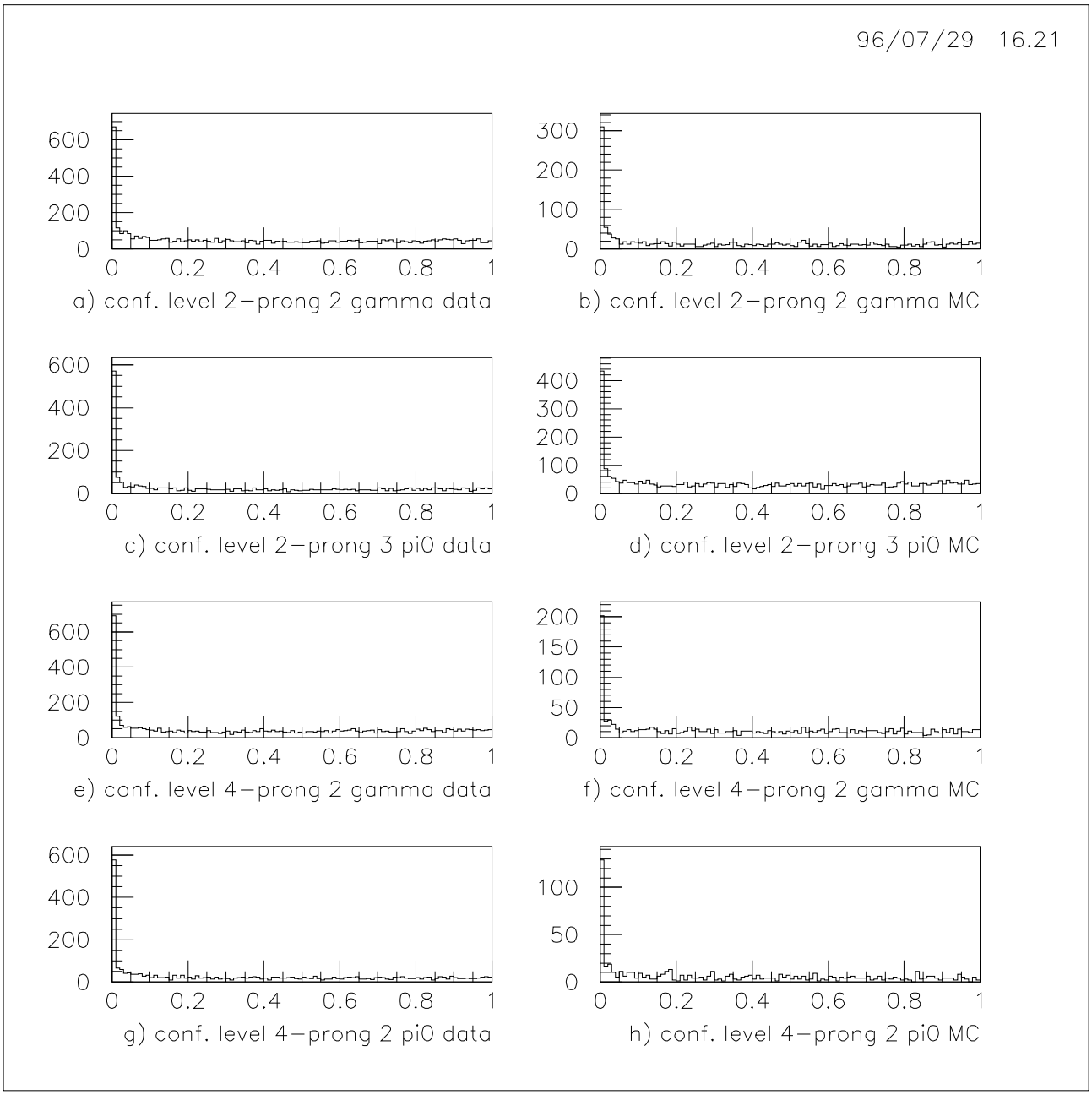

Figure 4: Confidence level distribution after the kinematic fit for 2 and 4-prong data and Monte Carlo for different number of photons.

	new JDC		old JDC	
Variable	2-prong data	Monte Carlo	4-prong data	Monte Carlo
$\sigma_{\sqrt{E}}$	1.3	1.1	1.3	1.18
σ_θ	1.15	1.2	1.2	0.87
σ_ϕ	1.05	0.9	1.05	0.74
$\sigma^+_{1/p_{xy}}$	1.15	0.81	1.7	1.0
$\sigma^+_{\tan\lambda}$	1.35	0.80	1.0	0.95
σ^+_ψ	0.9	0.64	0.72	0.65
$\sigma^-_{1/p_{xy}}$	1.15	0.81	1.7	1.0
$\sigma^-_{\tan\lambda}$	1.35	0.80	1.0	0.95
σ^-_ψ	0.9	0.64	0.72	0.65

Table 9: Scaling of the covariance matrix.

4 Decay distribution of $\eta' \to \pi^+\pi^-\gamma$

Of particular interest in this decay is the distribution of the $m(\pi^+\pi^-)$ invariant mass. This decay spectrum is determined by the following procedure:

First events are selected according to the cuts described in section 3.2 (page 5). The events were kinematically fitted and sorted in the following categories:

(1) $\overline{p}p \to \pi^0\gamma\pi^+\pi^-\gamma$

(2) $\overline{p}p \to \pi^0\pi^0\pi^+\pi^-\gamma$

(3) $\overline{p}p \to \pi^+\pi^-\pi^+\pi^-\gamma$

(4) $\overline{p}p \to \pi^+\pi^-\pi^0\pi^+\pi^-\gamma$

Then one can plot the $m(\pi^+\pi^-\gamma)$ invariant mass in bins of different $m(\pi^+\pi^-)$ mass intervals. From fits to the η' signal one gets a background independent number of the η''s versus the $m(\pi^+\pi^-)$ mass. Depending on the reaction this mass is selected by these cuts:

In reaction (1) the invariant $m(\pi^+\pi^-\gamma)$ mass was plotted, if

- $740 < m(\pi^0\gamma) < 830$ MeV for the recoiling combination,
- $m(\gamma\gamma) < 530$ or $m(\gamma\gamma) > 570$ MeV,
- the confidence level for the reaction $\overline{p}p \to \pi^0\pi^0\pi^+\pi^-$ was lower than 1%.

Reaction (2) required for the $m(\pi^+\pi^-\gamma)$ invariant mass plot that,

- $m(\pi^0\gamma) < 760$ or $m(\pi^0\gamma) > 805$ MeV for both combinations and
- $m(\pi^+\pi^-\pi^0) < 760$ or $m(\pi^+\pi^-\pi^0) > 805$ MeV for both combinations.

Reaction (3) did not need any further cuts, but all 4 $\pi^+\pi^-$ combinations were taken into account.

Reaction (4) had the same 4 $\pi^+\pi^-$ combinations. Additionally the recoiling invariant mass must form an ω: $740 < m(\pi^+\pi^-\pi^0) < 830$ MeV.

These cuts are illustrated in Figs. 5-8.

The relevant part of the $m(\pi^+\pi^-)$ invariant mass was cut into 25 MeV bins from 425 to 875 MeV. For each of these mass ranges an η' was fitted to the $m(\pi^+\pi^-\gamma)$ mass. In these fits the mass and width of the η' was fixed. Its values came from a global fit in the $550 < m(\pi^+\pi^-) < 850$ range. The fit function is a Gaussian with a Legendre background parameterization of degree 4 (See ''`http://nsdssp.lbl.gov/macro/gfit.kumac`''). The number of fitted η''s does not much depend on the mass and the degree of the Legendre polynomial. However there is a slight dependency on the width. Systematics were checked by doubling the $m(\pi^+\pi^-)$ bins from 25 to 50 MeV width. These yield the same number of η''s. This is not true, if the width of the η' is wrong. As another test the fit was performed by varying the width by $+3\sigma$ and -3σ. This varies the number of entries in the fitted signal by less than 1.2σ of the fit error.

Examples for these fits are shown in Fig. 9. The result of all fits are shown in Fig. 11.

The efficiency is calculated by performing the same fits to Monte Carlo datasets and dividing the number by the original generated events for each $m(\pi^+\pi^-)$ mass bin (see Fig. 10).

The final results are obtained after dividing the fitted signal by the efficiency for every mass bin. This is done independently for all four production reactions. The results are combined by a standard weighted least square procedure for each bin:

$$r \pm \sigma_r = \frac{\sum_k w_k f_k}{\sum_k w_K} \pm (\sum_k w_k)^{-1/2},$$

where

$$w_k = 1/(\frac{\sigma_{N_k}}{N_k} f_k)^2,$$

$$f_k = N_k / \sum_{bins} N_k,$$

$k = 1,4$ (reactions), N_k is the efficiency corrected signal for reaction k and a specific bin, σ_{N_k} its measurement error. f_k are the normalized signals and w_k are the weights.

The results r are tabulated in Table 10 and shown in Fig. 12.

$m(\pi^+\pi^-)$	relative rate
425 - 450 MeV	1.3 ± 0.6
450 - 475 MeV	1.6 ± 0.5
475 - 500 MeV	0.4 ± 0.6
500 - 525 MeV	2.2 ± 0.6
525 - 550 MeV	2.0 ± 0.6
550 - 575 MeV	3.0 ± 0.6
575 - 600 MeV	4.1 ± 0.6
600 - 625 MeV	4.5 ± 0.6
625 - 650 MeV	6.5 ± 0.6
650 - 675 MeV	8.4 ± 0.7
675 - 700 MeV	10.0 ± 0.7
700 - 725 MeV	13.4 ± 0.8
725 - 750 MeV	15.6 ± 0.8
750 - 775 MeV	15.8 ± 0.8
775 - 800 MeV	9.3 ± 0.6
800 - 825 MeV	7.4 ± 0.5
825 - 850 MeV	2.2 ± 0.5
850 - 875 MeV	0.4 ± 0.6

Table 10: Final results η' decay spectrum.

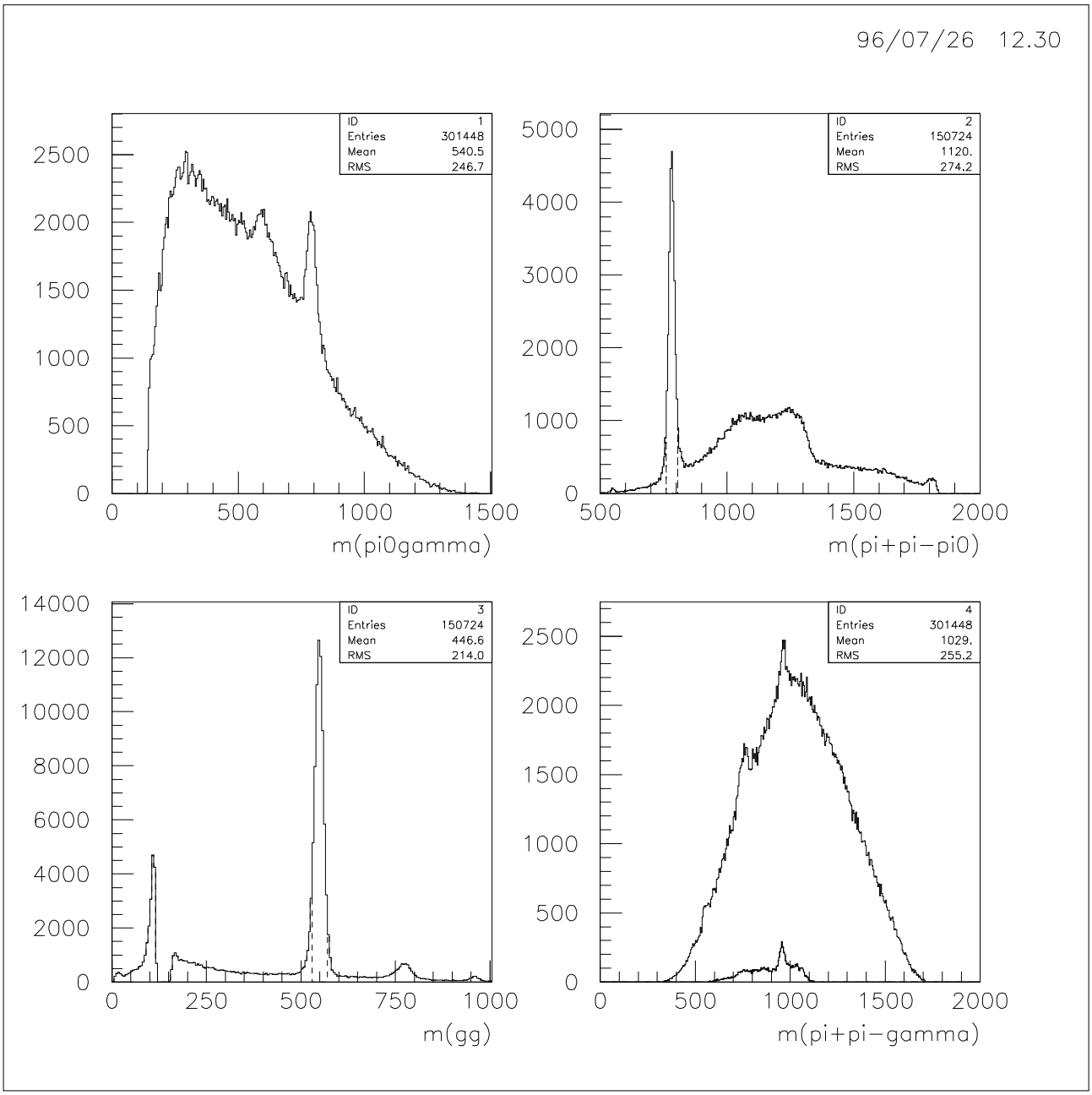

Figure 5: Reaction (1): Invariant $m(\pi^0\gamma)$ (a), $m(\pi^+\pi^-\pi^0)$ (b) and $m(\gamma\gamma)$ (c) masses width cuts drawn in (b) and (c). $m(\pi^+\pi^-\gamma)$ (d) before and after the cuts on (b) and (c).

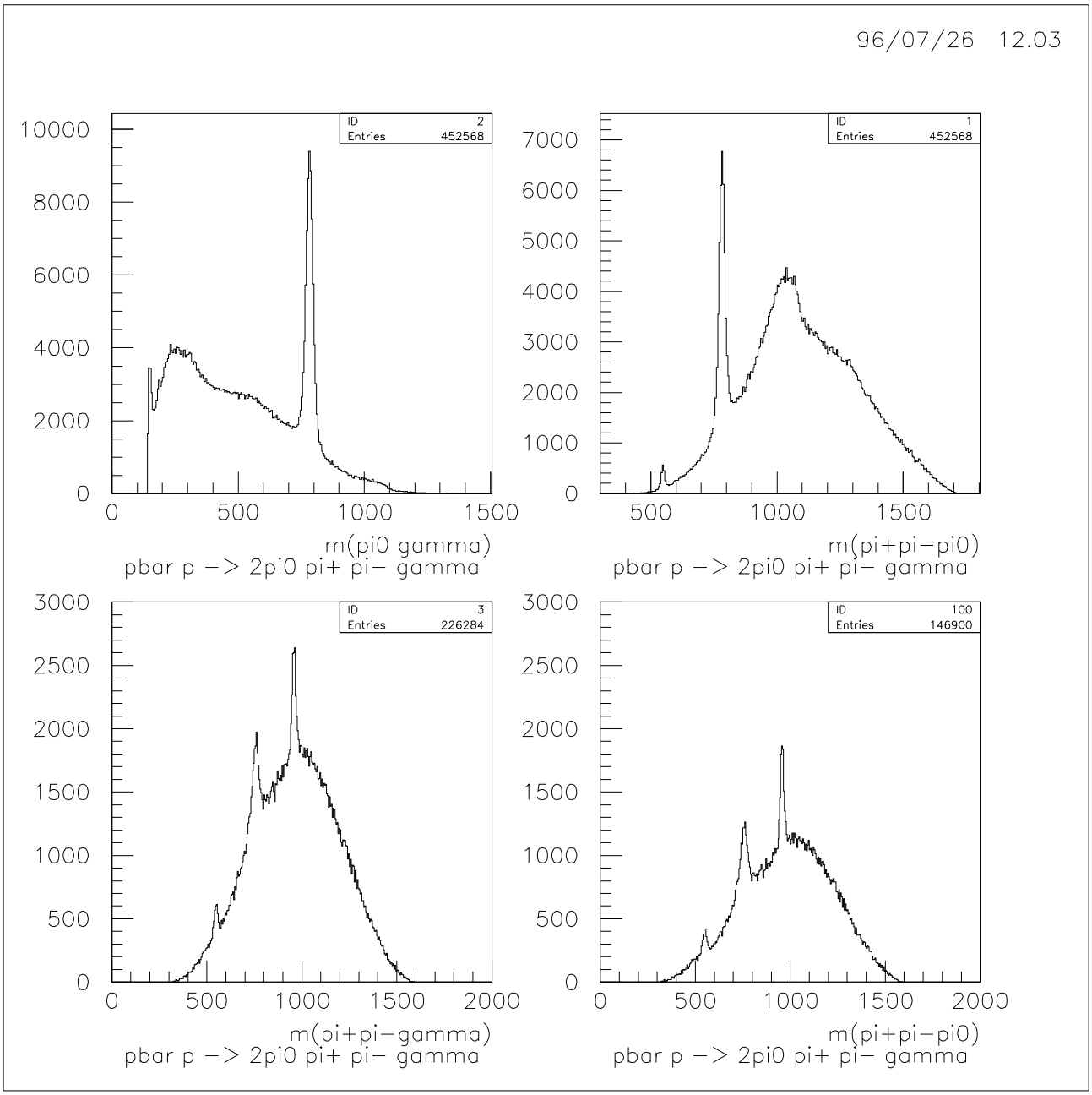

Figure 6: Reaction (2): Invariant $m(\pi^0\gamma)$ (a), $m(\pi^+\pi^-\pi^0)$ (b) and $m(\pi^+\pi^-\gamma)$ (c) masses before cuts and $m(\pi^+\pi^-\gamma)$ (d) after the cuts on (a) and (b).

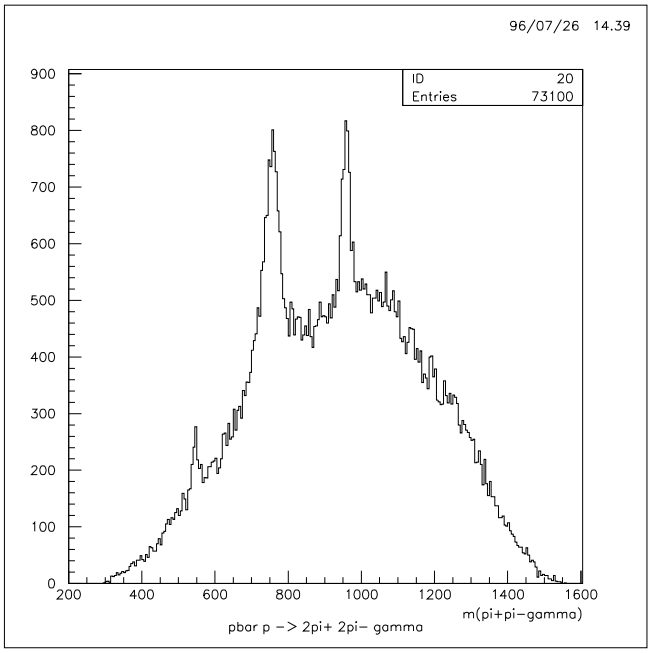

Figure 7: Reaction (3): Invariant $m(\pi^+\pi^-\gamma)$ masses. Four entries/event.

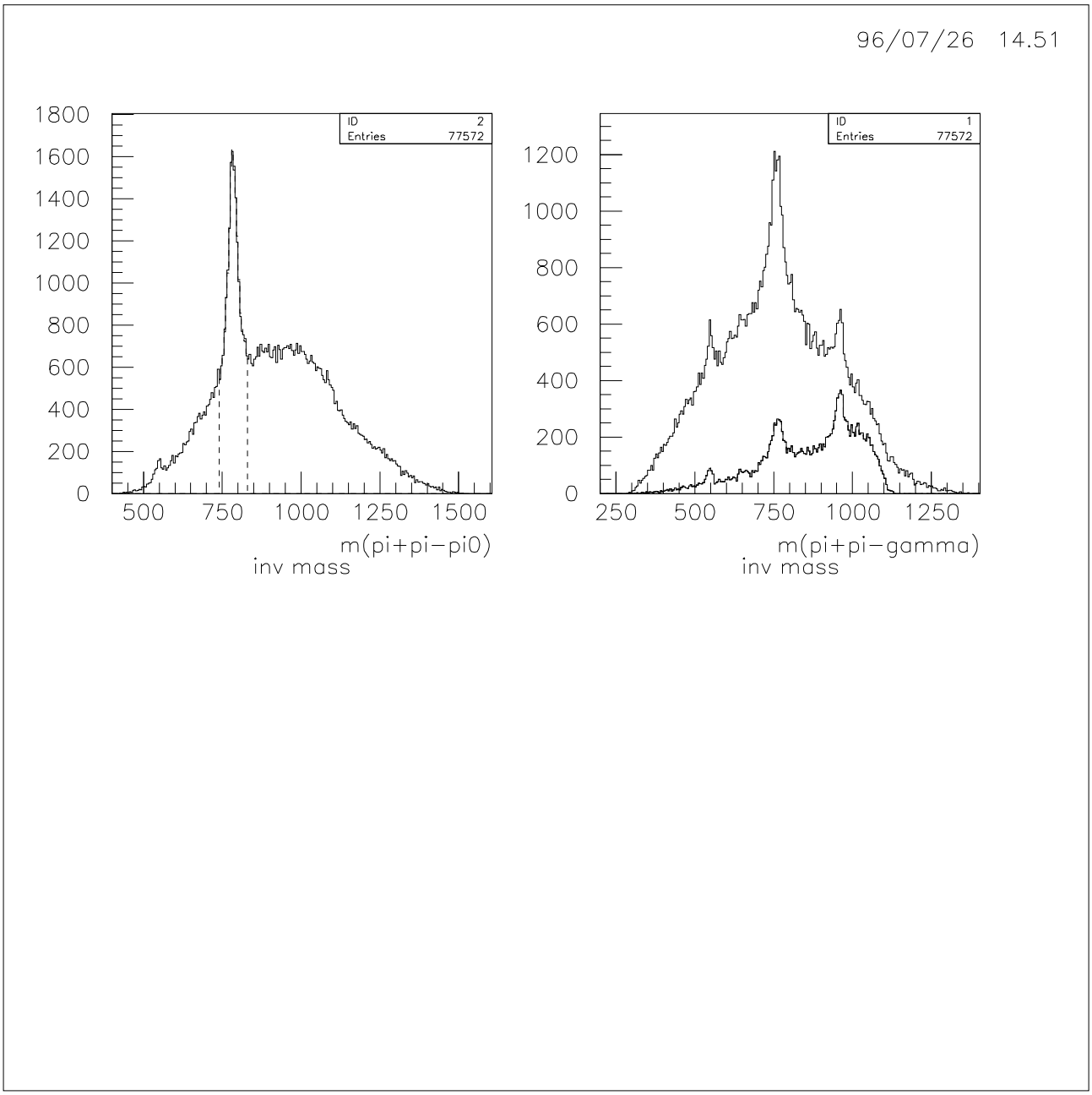

Figure 8: Reaction (4): Invariant $m(\pi^+\pi^-\pi^0)$ mass (a) and $m(\pi^+\pi^-\gamma)$ (b) before and after the cuts on (a).

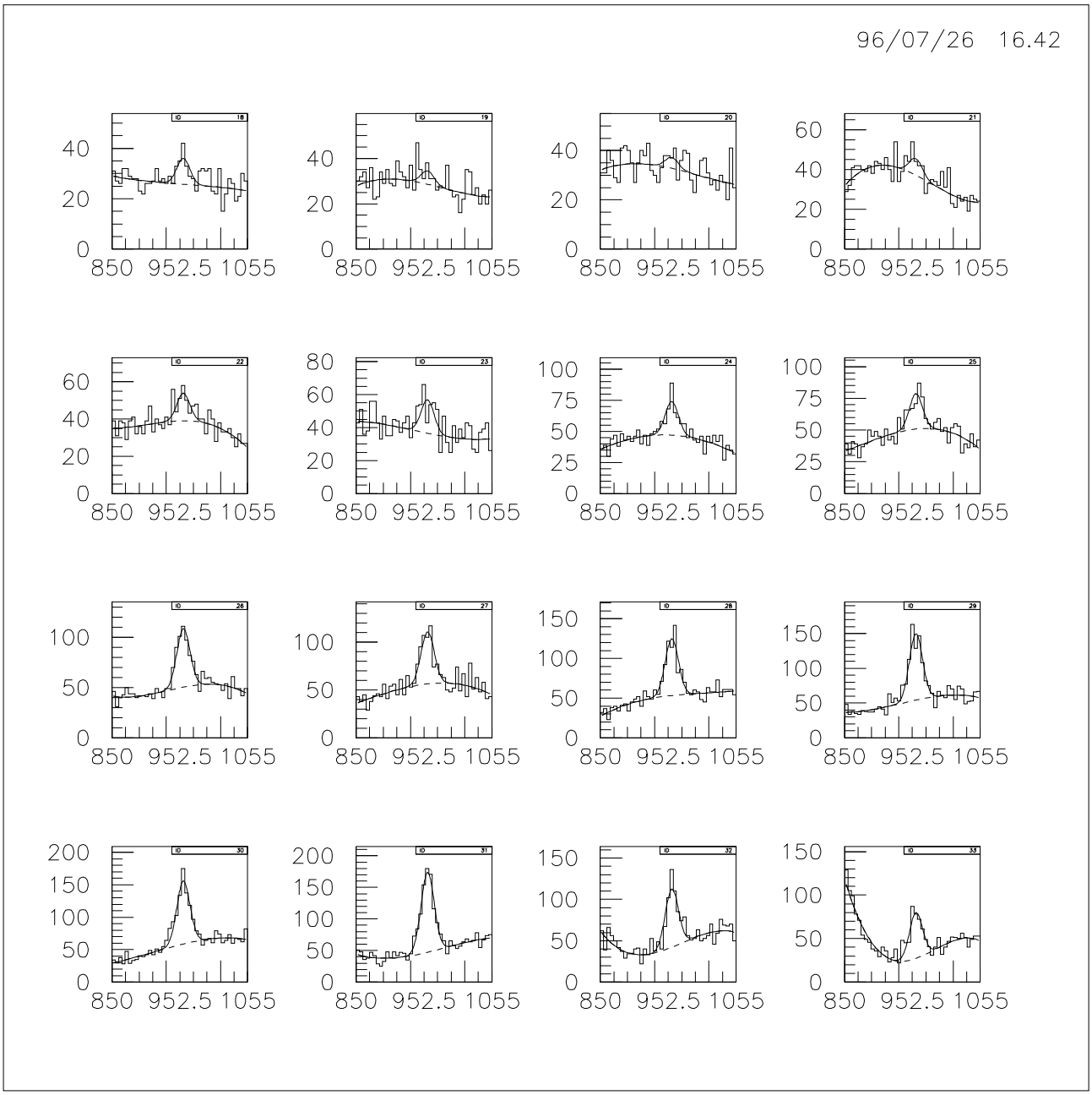

Figure 9: $m(\pi^+\pi^-)$ distribution in the $m(\pi^+\pi^-)$ bins from 425 to 825 MeV (25 MeV steps). Shown for the reaction (2) $\overline{p}p \to \pi^0\pi^0\pi^+\pi^-\gamma$.

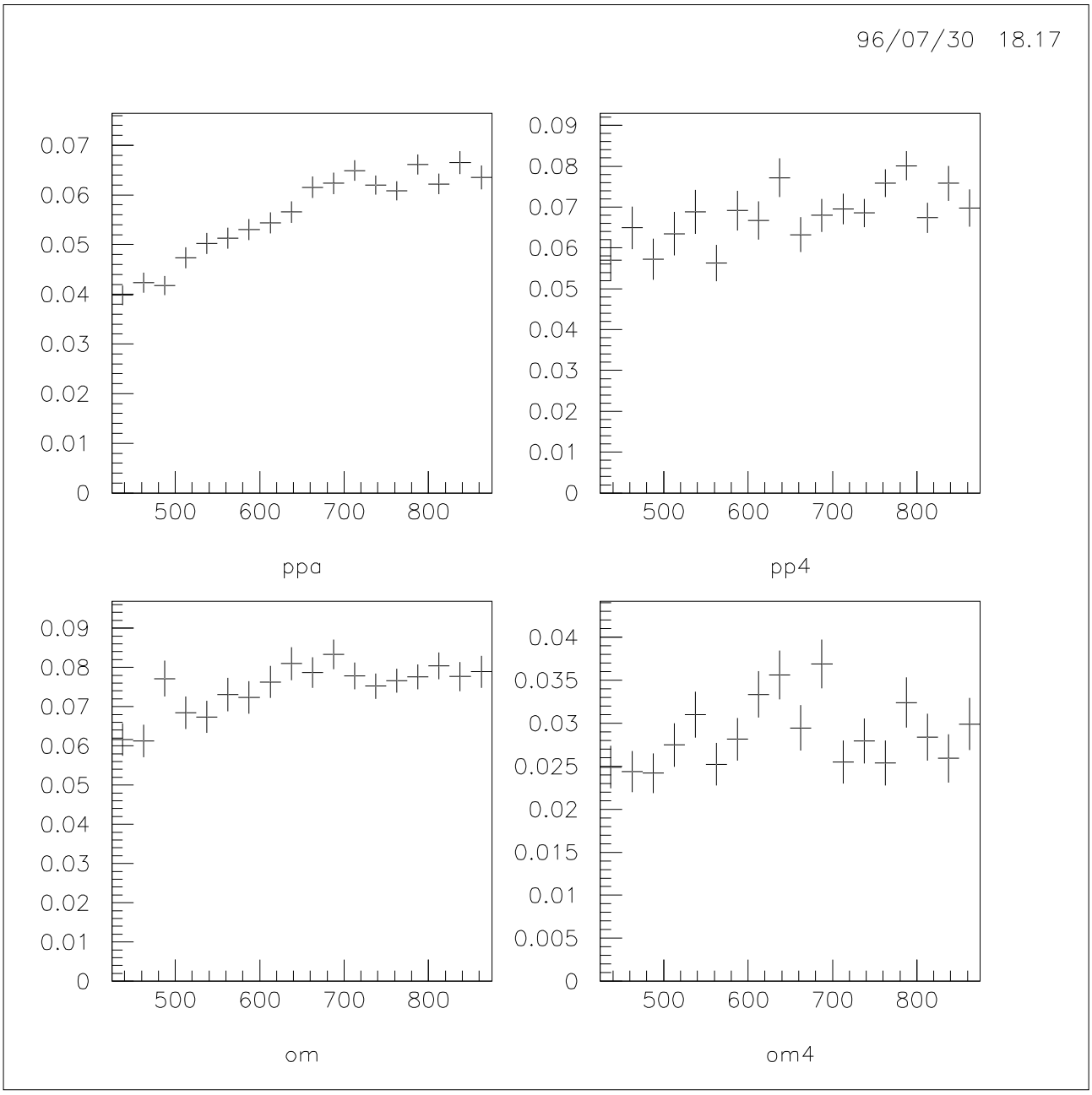

Figure 10: Efficiency versus $m(\pi^+\pi^-)$ for the decay $\eta' \to \pi^+\pi^-\gamma$. Results are shown for the 4 different reactions.

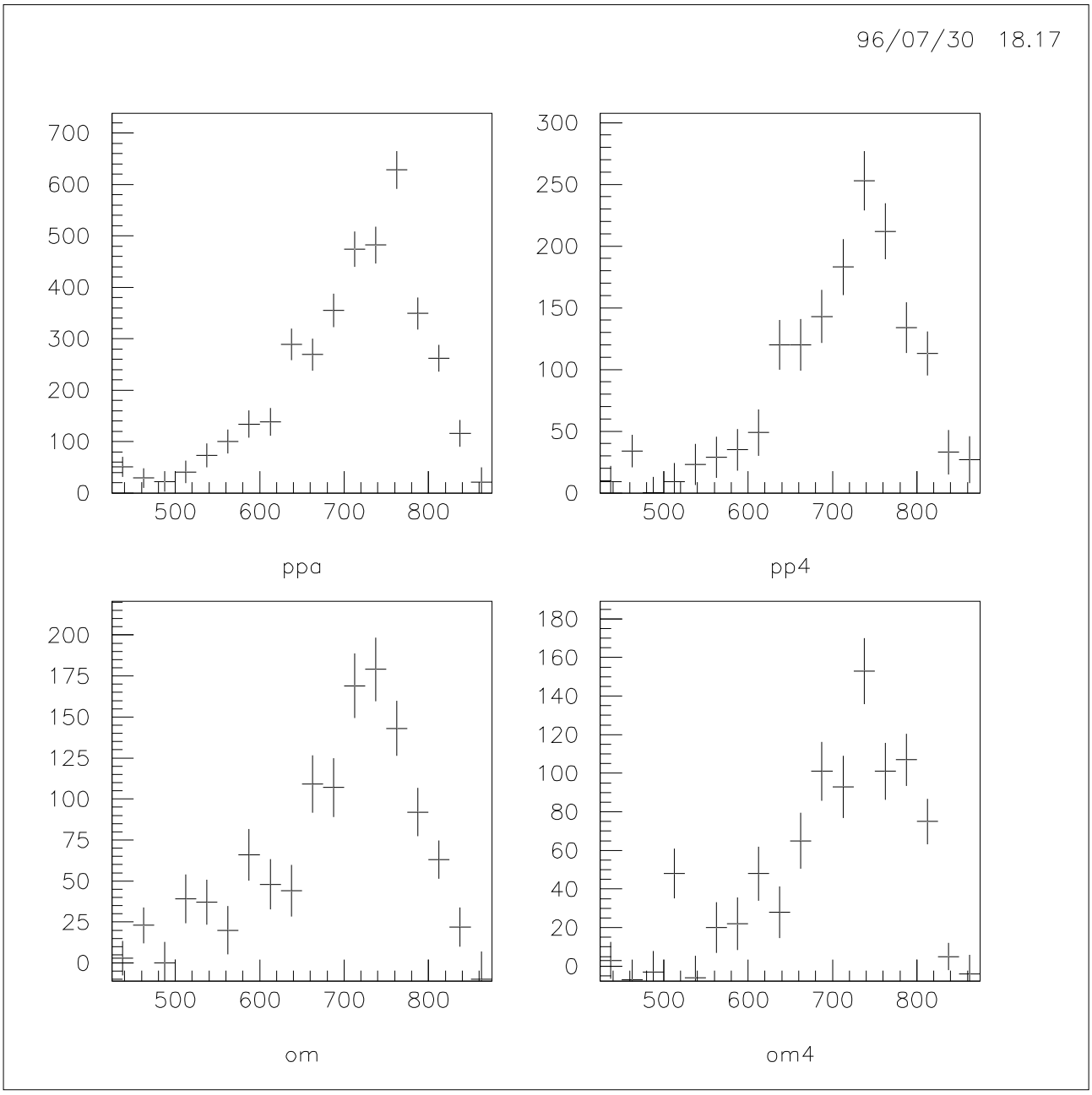

Figure 11: Fitted number of η' versus $m(\pi^+\pi^-)$ for the decay $\eta' \to \pi^+\pi^-\gamma$. Results are shown for the 4 different reactions.

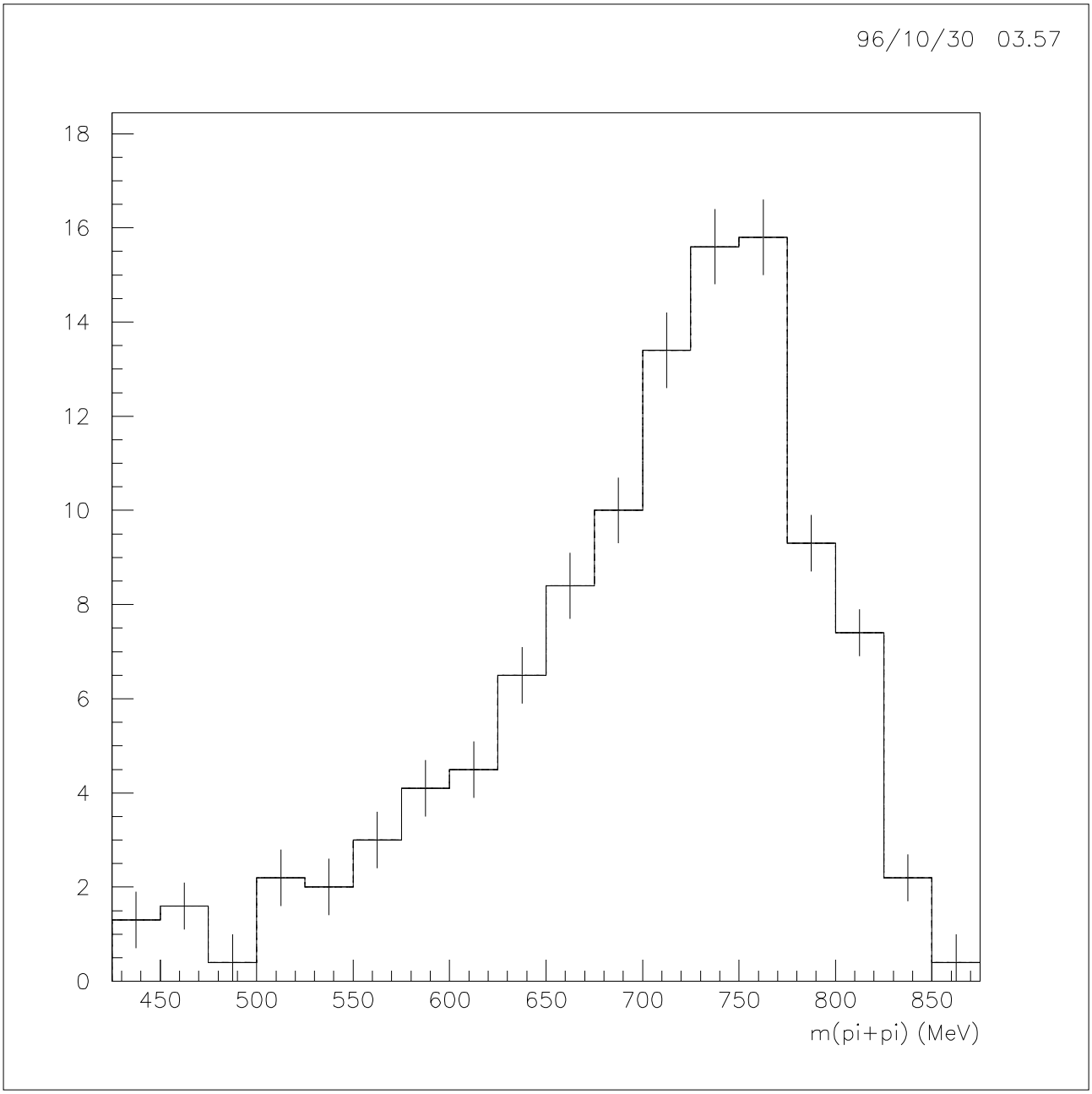

Figure 12: $m(\pi^+\pi^-)$ distribution in the decay $\eta' \to \pi^+\pi^-\gamma$.

5 Study of box anomaly in $\eta' \to \pi^+\pi^-\gamma$

5.1 Method to study the box anomaly in η/η' decays

The data set in table 10 is the tenth measurement of the $\pi^+\pi^-$ mass spectrum of the $\eta' \to \pi^+\pi^-\gamma$ decay. A full list of the previous measurements can be found in ref. [3]. These measurements rely on statistics running from about 200 events to about 2000 events ; altogether they amount to about 8000 events in 9 experiments with different systematic errors. Our sample (6910 events) represents therefore a doubling of the statistics by a single experiment. This allows for a consistent study of this mass spectrum in order to extract the box anomaly constant expected to exist beside the dominant ρ contribution and a check of its statistical significance.

Moreover, using our spectrum for $\eta' \to \pi^+\pi^-\gamma$ together with the two photon decay widths of the η and η' mesons, and the $\pi^+\pi^-$ mass spectrum of the $\eta \to \pi^+\pi^-\gamma$ decay [7], allows to perform a measurement of the pseudoscalar parameters (f_1, f_8 and θ_{PS}). This is done by means of the Chanowitz equations [1, 2] and of an equation (hereafter called AFN) on J/ψ radiative decays to η and η' [8, 9].

These five equations provide a test of QCD through the value of the Chanowitz parameter ξ ; if QCD holds, this parameter is expected to get 1 as value. Integral charge quark models [1, 2] favor a value of 2. The experimental input to these equations are the triangle anomaly constants (B_X, $X = \eta,\ \eta'$) which can be deduced algebraically from the two–photon decay widths of η and η' :

$$\Gamma(X \to \gamma\gamma) = \frac{M_X^3}{64\pi}|B_X|^2 \quad , \quad X = \eta,\ \eta' \quad , \tag{1}$$

The box anomaly constants (E_X, $X = \eta,\ \eta'$), can be deduced from fit to the $\pi^+\pi^-$ mass spectra in the decays $\eta/\eta' \to \pi^+\pi^-\gamma$ using :

$$\frac{d\Gamma_X}{dm} = \frac{1}{48\pi^3}\left|\frac{2G_\rho(m)F_X}{D_\rho(m)} + E_X\right|^2 k_\gamma^3 q_\pi^3 \quad , \tag{2}$$

with $k_\gamma = (M_X^2 - m^2)/2M_X$ and $q_\pi = 1/2\sqrt{m^2 - 4m_\pi^2}$. F_X is the coupling constant at the vertex $X\rho\gamma$ in the diagram representing the ρ contribution. The functions $G_\rho(m)$ and $D_\rho(m)$ are obtained from a fit [3] of all e^+e^- data [10]. More precisely, we have :

$$\begin{cases} D_\rho(m) = (m_\rho^2 - m^2) - im_\rho\Gamma_\rho(m) \\ \Gamma_\rho(m) = \Gamma_\rho(m_\rho)\left[\dfrac{q_\pi(m)}{q_\pi(m_\rho)}\right]^3\left[\dfrac{m_\rho}{m}\right]^\lambda \\ G_\rho(m) = \sqrt{6\pi\dfrac{mm_\rho}{q_\pi^3}\Gamma_\rho(m)} \end{cases} \tag{3}$$

m being the running dipion mass, $\Gamma_\rho(m)$ is the varying width of the ρ^0 meson, $D_\rho(m)$ its propagator and $G_\rho(m)$ its coupling to the $\pi^+\pi^-$ final state. λ is a damping power describing the fall–off of the ρ broad peak.

From equation (2), one clearly sees that any direct measurement of the box anomalies strongly relies on the model used to describe the ρ meson. Two models of the ρ meson will be used in the following. They have been described in ref. [3]. One is called M_2 and fulfills the

	Model M_1	Model M_2
m_ρ (MeV)	**769.1 ± 0.9**	$780.8^{+0.5}_{-0.4}$
Γ_ρ (MeV)	$142.8^{+1.5}_{-2.4}$	153. ± 2.
λ	1.748 ± 0.079	0.659 ± 0.046
χ^2/dof	61/77	90/78

Table 11: Parameter values in the fit of the $e^+e^- \to \pi^+\pi^-$ cross section ; numerical values written boldface are fixed (input) values taken from PDG. The first two parameters are the mass and width of the ρ^0 meson, λ is the damping power affecting the ρ^0 high–mass tail. The last line gives the fit quality obtained in fitting the $e^+e^- \to \pi^+\pi^-$ cross section.

requirements of VDM in describing the annihilation process $e^+e^- \to \pi^+\pi^-$. The other named M_1 assumes the existence in this last process of a VDM violating contribution by allowing a non–resonant coupling $\gamma\pi^+\pi^-$. Such kinds of coupling are allowed in recent formulations of chiral theories [11, 12]. Moreover, Chung *et al* [13] have shown that the quark structure of the pion is able to generate such non–resonant coupling in the charged pion form factor. Chiral theories provide a constant non–resonant coupling while the result of Chung *et al* shows in a likely way that this term can be mass dependent as for model M_1 (see rels.(13–14) in ref. [3]). We have discarded other kinds of models for the ρ meson like the Gounaris–Sakurai model [14], as it has been shown that its description of e^+e^- data is not satisfactory without additional assumptions (see ref. [10]).

Therefore, in order to perform our fits, we shall use two parameterizations of the ρ meson. They are summarized in Table 11. From a statistical point of view, all these parameterizations give a good description of the e^+e^- data.

As mentioned just above, a direct extraction of the box anomaly constant from data is strongly dependent on the assumptions done about the ρ mass distribution. However, one can find numerical predictions for the box anomaly constants which are independent of any assumption about the ρ meson. This allows us to find by consistency which assumption about the ρ meson is likely to be the right one.

Indeed, the two Chanowitz equations involving the triangle anomalies for η and η' (see rels. (A . 1) in the appendix) only rely on the the two–photon decay widths of these two mesons (see rel. (1) above). On the other hand, the AFN equation (see rel. (A . 3) in the appendix) only relies on the radiative decays of the J/ψ meson to η and η'. We have then 3 equations relating 3 unknowns (f_1, f_8, θ_{PS}) for each expected value of ξ (= 1 or 2). Having solved these three equations for both ξ values, allows to predict the box anomaly constant values using eqs (A . 2) from appendix. These predictions are obviously independent of any assumption on the ρ meson parameterization and can be compared with the values extracted from data. This computation has been done in ref. [4] and gives :

$$\begin{cases} E_{\eta'} = -5.32 \pm 0.18 \quad , \quad E_\eta = -6.84 \pm 0.31 \quad , \quad (\xi = 1) \\ E_{\eta'} = -2.05 \pm 0.13 \quad , \quad E_\eta = -4.41 \pm 0.23 \quad , \quad (\xi = 2) \end{cases} \tag{4}$$

where all numbers are given in units of GeV^{-3}. The predictions displayed in rel. (4) are our

reference values and one should stress that they are independent of any assumption about the ρ meson.

5.2 Fit of η' box anomaly

In fact, all published $\pi^+\pi^-$ mass spectra from η/η' decays to $\pi^+\pi^-\gamma$ are not given in absolute magnitude, as our own spectrum from table 10 above. Therefore equation (2) has to be multiplied by an arbitrary normalization. As a matter of consequence, we are not sensitive to $E_{\eta'}$ and $F_{\eta'}$ separately, but only to their ratio.

As soon as a value of E_X/F_X is obtained from a minimization procedure the value of F_X is simply given by :

$$\frac{1}{F_X^2} = \frac{1}{\Gamma(X \to \pi^+\pi^-\gamma)} \frac{1}{48\pi^3} \int_{2m_\pi}^{M_X} \left| \frac{2G_\rho(m)}{D_\rho(m)} + \frac{E_X}{F_X} \right|^2 k_\gamma^3 q_\pi^3 dm \quad , \tag{5}$$

using our fitted ratio and the width to $\pi^+\pi^-\gamma$ given in the PDG. Another relation gives $1/E_X^2$ in terms of measured quantities ; it is simply obtained by multiplying relation (4) by $(F_X/E_X)^2$.

	Model M_1	Model M_2
$E_{\eta'}/F_{\eta'}$	-13.05 ± 1.19	-5.32 ± 1.19
$E_{\eta'}$	-5.38 ± 0.50	-2.22 ± 0.53
$F_{\eta'}$	0.41 ± 0.03	0.43 ± 0.03
χ^2/dof	26/17	26/17
E_η/F_η	$-10.64^{+2.49}_{-2.07}$	$+13.48^{+3.80}_{-3.25}$
E_η	$-4.39^{+1.15}_{-1.00}$	$-3.64^{+1.10}_{-0.97}$
F_η	0.41 ± 0.05	-0.27 ± 0.03
χ^2/dof	13/14	8/14

Table 12: Values of the fitting parameter E_X/F_X and the corresponding values for E_X and F_X. In the case of η', the fit is done using only the Crystal Barrel data ; in the case of η, the fit is performed using only the data of Layter *et al* from ref. [7]. All values of E_X are in units of GeV^{-3}, while all values of F_X are in units of GeV^{-1}.

The absolute values of F_X and E_X can be obtained with their errors from rel. (5) by making a sampling of the measured quantities (the width and the E/F ratio, the ρ parameters $\cdots$) considering their central values as mean values of random gaussian distributions and their errors

as the corresponding standard deviations. Finally, it has been shown in ref. [3] that the sign for each box anomaly constant must be chosen negative. All following results will take this remark into account.

The fit of the dipion spectrum in $\eta' \to \pi^+\pi^-\gamma$ has been performed with the two models for the ρ meson described above. The results are collected in the upper part of table 12 and exhibit the same (and good) fit probability. A typical fit is shown in fig 13. The values obtained for $E_{\eta'}$ are in good agreement with expectations (see rel. 4) and show that model M_2 tends to favor $\xi = 2$, while model M_1 tends to favor $\xi = 1$.

Our results show that the value for $E_{\eta'}$ is 10 or 4 σ away from 0. Therefore, our data confirm the existence of the box anomaly in η' decay to $\pi^+\pi^-\gamma$ at a level consistent with predictions from Chanowitz [1, 2] and AFN [9] equations.

We also give for further use the results of fitting the corresponding spectrum [7] coming from $\eta \to \pi^+\pi^-\gamma$ decay (see also ref. [3, 4]).

5.3 The pseudoscalar nonet parameters

Using the η/η' two–photon decay widths, the J/ψ radiative decay widths to η/η' both from PDG, and the box anomaly constants obtained from fit to Crystal Barrel and Layter [7] data, we have an estimate of the left–hand sides of the five equations given in the appendix. These equations depends on four or three parameters, depending on whether one leaves free or fixed (to 1 or 2) the unknown ξ. Therefore, we can solve these equations in order to get an estimate of the pseudoscalar nonet parameters f_1, f_8, θ_{PS}, and subsequently of ξ.

The results with fixed values of ξ are given in table 13.

	Model M_1	Model M_2
ξ (fixed)	1	2
χ^2/dof	5.40/2	0.9/2
$\frac{f_\pi}{f_1}$	0.91 ± 0.02	0.48 ± 0.01
$\frac{f_\pi}{f_8}$	0.89 ± 0.05	0.60 ± 0.04
θ_{PS}	$-16.2° \pm 1.2°$	$-23.1° \pm 1.3°$
χ^2/dof (converse ξ)	40/2	41/2

Table 13: Values of the pseudoscalar nonet parameters obtained by fitting the η and η' mass spectra using the quoted ρ^0 model.

This table clearly shows that the ρ model M_2 (in full agreement with VDM) is inconsistent with the QCD prediction that $\xi = 1$; model M_1 allowing a VDM violating term permits

to recover the QCD prediction ($\xi = 1$). The probability for the former model is above the 80% level, the probability for the latter is about 15% which is still acceptable. Therefore this new η' data set confirms the ambiguity already noticed [3, 4].

If we leave free the parameter ξ in our minimization procedure, we get :

$$\begin{cases} \xi = 1.05 \pm 0.08 & (\chi^2/dof = 4.96/1) \quad \text{Model } M_1 \\ \xi = 2.05^{+0.40}_{-0.29} & (\chi^2/dof = 0.88/1) \quad \text{Model } M_2 \end{cases} \tag{6}$$

which confirms our previous conclusion.

From table 13, one clearly sees that model M_1 favours the nonet symmetry in the pseudoscalar sector ($f_1 = f_8$) and find a mixing angle close to a previous determination from the Crystal Barrel Collaboration [15]. Model M_2 finds a small breaking of nonet symmetry ($\simeq 20\%$), but gets the mixing angle at a value expected from SU(3) mass formulae.

5.4 Conclusion

The $\pi^+\pi^-$ mass spectrum in the decay $\eta' \to \pi^+\pi^-\gamma$ has been measured with the Crystal Barrel detector. It allows to confirm the existence of the box anomaly with a statistical significance of more than 4 σ.

Using other data from PDG (the two–photon decay widths of the η and η' mesons and the radiative decay widths of J/ψ to η and η'), the spectrum measured by Layter *et al* [7] in the η decay and our own spectrum for the η' decay, we give a measurement of the pseudoscalar nonet parameters.

There remains an ambiguity due to the correct ρ model which cannot be solved with our data on a statistical basis. However, our results tends to show that the VDM assumption leads to an inconsistency with QCD. They also show that the existence of a non–resonant coupling $\gamma\pi^+\pi^-$, by modifying the ρ shape, allows to recover an agreement between data and the QCD prediction that $\xi = 1$. This coupling however must be mass dependent.

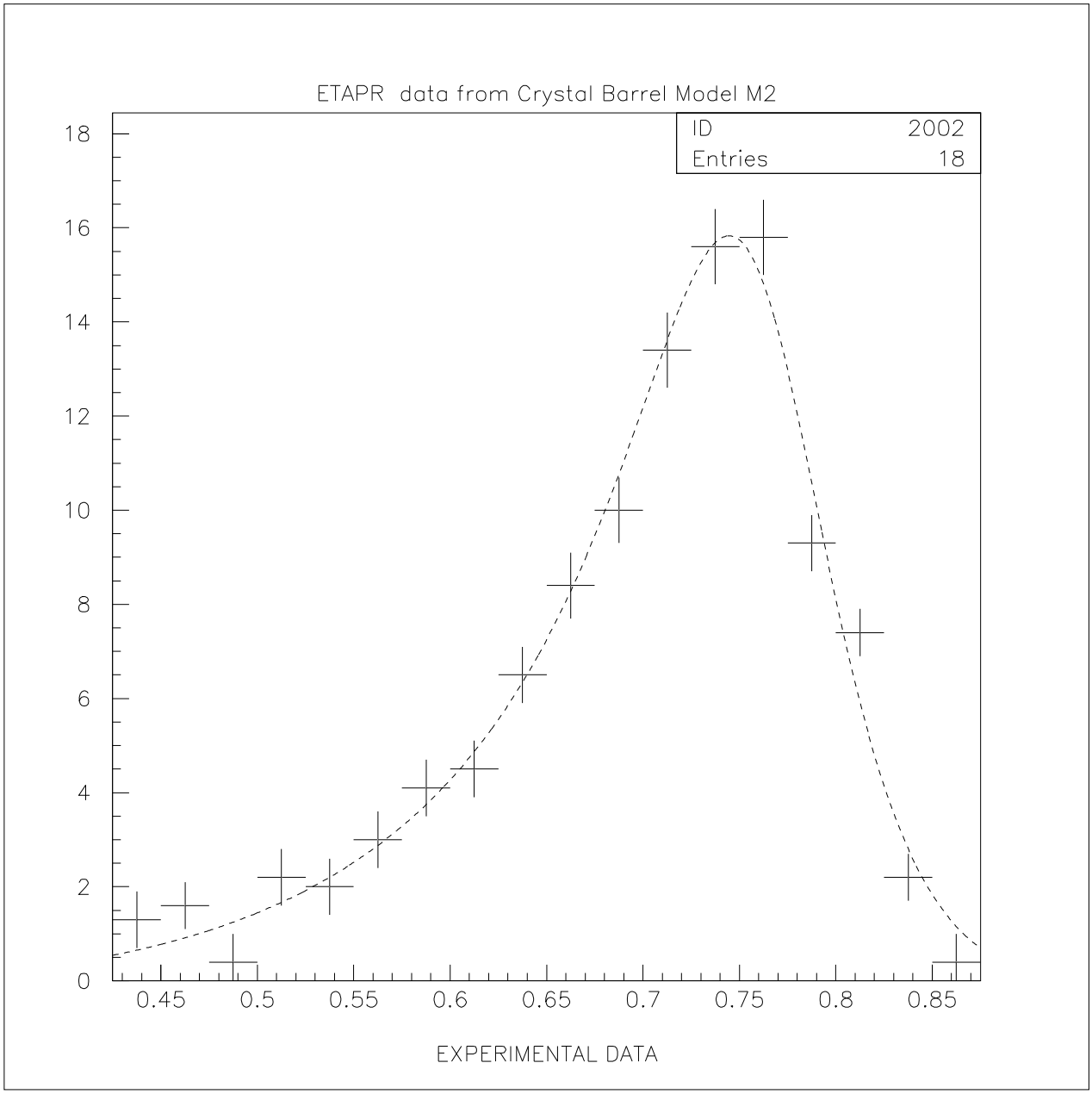

Figure 13: $m(\pi^+\pi^-)$ distribution in the decay $\eta' \to \pi^+\pi^-\gamma$. Crystal Barrel data is shown as crosses together with the result of the fit with model M_2 (dashed line).

6 Analysis of the Dalitz plot $\eta \to \pi^+\pi^-\pi^0$

The events of the type $\eta \to \pi^+\pi^-\pi^0$ were subject to a Dalitz plot analysis of the η decay mode $\pi^+\pi^-\pi^0$. The matrix element depends mainly on $s = (p_\eta - p_{\pi^0})^2$. When using standard Dalitz plot variables

$$x = \sqrt{3}\frac{T_+ - T_-}{Q} = \frac{\sqrt{3}}{2m_\eta Q}(u - t),$$

$$y = \frac{3T_0}{Q} - 1 = \frac{3}{2m_\eta Q}\{(m_\eta - m_{\pi^0})^2 - s\} - 1,$$

$$Q = m_\eta - 2m_{\pi^+} - m_{\pi^0}$$

the main dependence is on y. In the latter only the projection of the Dalitz plot to the y axes is analyzed.

The selection and analysis method used is the same as the one for the η' decay analysis.

A kinematical fit to the reaction

$$\overline{p}p \to \pi^+\pi^-\pi^0\pi^0\pi^0$$

yields 3329 events of the type $\overline{p}p \to \pi^0\pi^0\eta$, $\eta \to \pi^+\pi^-\pi^0$.

Using all three $\pi^+\pi^-\pi^0$ combinations the $m(\pi^+\pi^-\pi^0)$ invariant mass is histogrammed in the 19 different y bins in the possible range of $y = -1.0 \ldots 0.9$. Whereas y is calculated according to:

$$y = \frac{3T_0}{T_+ + T_- + T_0} - 1$$

with T_0, T_+ and T_- the kinematic energy of the π^0, π^+ and π^- in the restframe of the $\pi^+\pi^-\pi^0$ system, respectively. In the fits the mass of the η was fixed to the value determined by fitting the full spectrum (see Fig. 14). The efficiency was determined by applying the same method to a sample of 140000 Monte Carlo events (Fig. 15).

The dependence of the matrix-element squared from the variable y can be seen after the normalization to the phase space, which was calculated using Mathematica.

6.1 Integrated phasespace over y bins

The contribution of every part of the Dalitz plot between y_1 and y_1 was calculated by integrating over phase space:

$$\int_{y_1}^{y_2} \frac{\sqrt{3}}{2m_\eta Q}\left\{\left(\sqrt{E_1(y)^2 - m_{\pi^\pm}^2} + \sqrt{E_3(y)^2 - m_{\pi^0}^2}\right)^2 - \left(\sqrt{E_1(y)^2 - m_{\pi^\pm}^2} - \sqrt{E_3(y)^2 - m_{\pi^0}^2}\right)^2\right\} dy$$

where

$$E_1(y) = \frac{\sqrt{s(y)}}{2},$$

$$E_3(y) = \frac{m_\eta^2 - m_{\pi^0}^2 - s(y)}{2\sqrt{s(y)}},$$

$$s(y) = (m_\eta - m_{\pi^0})^2 - \frac{(1+y)2m_\eta Q}{3}.$$

The contributions of the different y bins to the phase space is listed in Table 14 and shown in Fig. 15.

y-range	phasespace
-1.0 – -0.9	0.0160383
-0.9 – -0.8	0.0291854
-0.8 – -0.7	0.0375551
-0.7 – -0.6	0.0441244
-0.6 – -0.5	0.0495718
-0.5 – -0.4	0.0541824
-0.4 – -0.3	0.0580959
-0.3 – -0.2	0.0613801
-0.2 – -0.1	0.0640592
-0.1 – 0.0	0.066125
0.0 – 0.1	0.067541
0.1 – 0.2	0.0682397
0.2 – 0.3	0.0681157
0.3 – 0.4	0.0670108
0.4 – 0.5	0.0646837
0.5 – 0.6	0.0607484
0.6 – 0.7	0.0545206
0.7 – 0.8	0.0445197
0.8 – 0.9	0.0243035

Table 14: Phasespace distribution

6.2 Fits to the Matrix element

The measured distribution of $M^2(y)$ can be seen in Figure 16. For later reference the data is also tabulated in Table 15. The distribution was fitted to the function:

$$M^2(y) = N(1 + ay + by^2) \tag{7}$$

In a second fit the parameter b was fixed to 0 to allow a better comparison to one experiment which did the same. The data is also tested against the parameterization of two other experiments and two theoretical predictions. The fit results are listed together with other experimental and theoretical values in table 16. The χ^2 values show a clear agreement of the CBAR data with the other two experimental results and with the chiral perturbation theory expectation. However the current algebra prediction, which is equivalent to the first order term of chiral perturbation theory is rejected by the data.

Following a procedure given in [6] one can calculate the value

$$r = \frac{\mathrm{BR}(\eta \to 3\pi^0)}{\mathrm{BR}(\eta \to \pi^+\pi^-\pi^0)}$$

from the parameterization of the matrix element $M^2(y) = N(1 + ay + by^2)$. Results are shown in the last column of table 16. All experiments are compatible with the chiral perturbation prediction and the result of the direct measurements from the particle data group averages of $r = 1.34 \pm 0.10$ and the global fit of $r = 1.39 \pm 0.04$ [16].

Although the dependence of M^2 on x was not measured in this experiment, one can still compare the distribution to the function

$$M^2(x, y) = N(1 + ay + by^2 + cx^2). \tag{8}$$

The results are given in table 17. Because the fit of c is not very meaningful (see first line of the table), the value of c was fixed to values obtained from theory or other experiments. The values of a and b are mostly independent from c within the observed range of c.

y range	$M^2(y)$
-1.00 – -0.90	1.00 ± 0.13
-0.90 – -0.80	0.73 ± 0.08
-0.80 – -0.70	0.88 ± 0.09
-0.70 – -0.60	0.73 ± 0.07
-0.60 – -0.50	0.67 ± 0.06
-0.50 – -0.40	0.64 ± 0.06
-0.40 – -0.30	0.67 ± 0.07
-0.30 – -0.20	0.56 ± 0.05
-0.20 – -0.10	0.41 ± 0.05
-0.10 – -0.00	0.43 ± 0.04
-0.00 – 0.10	0.37 ± 0.04
0.10 – 0.20	0.30 ± 0.04
0.20 – 0.30	0.28 ± 0.03
0.30 – 0.40	0.23 ± 0.04
0.40 – 0.50	0.27 ± 0.04
0.50 – 0.60	0.14 ± 0.02
0.60 – 0.70	0.14 ± 0.03
0.70 – 0.80	0.10 ± 0.02
0.80 – 0.90	0.03 ± 0.03

Table 15: Table of the phase space normalized projection of the $\eta \to \pi^+\pi^-\pi^0$ Dalitz plot on to the y-axes.

Experiment	a	b	χ^2/N	r
CBAR (b fixed)	-1.10 ± 0.04	0	17.2/17	1.430 ± 0.014
CBAR	-1.19 ± 0.07	0.19 ± 0.11	14.1/16	1.441 ± 0.042
Layter et al.[7]	-1.07±0.013	0	17.7/18	1.440 ± 0.005
Gormley et al.[17]	-1.18±0.02	0.20±0.03	14.3/18	1.446 ± 0.012
Theory	a	b		
Current Algebra	-1.01	0.26	43.9/18	1.51
χPT [6]	-1.30	0.38	16.8/18	1.43±0.03

Table 16: Parameter for the distribution $M^2(y) = N(1+ay+by^2)$. The χ^2/N value is given for a fit to the CBAR data of the specified functions. For the fits to the other experiments and the theory no errors in a and b are taken into account. In the last column the r value calculated from the matrix element $M^2(y) = N(1 + ay + by^2)$ is given. See text.

Experiment	a	b	c	χ^2/N
CBAR	-1.17 ± 0.39	0.17 ± 0.42	-0.05 ± 0.99	14.1/15
CBAR (c fixed)	-1.21 ± 0.07	0.21 ± 0.11	0.046	14.1/16
CBAR (c fixed)	-1.22 ± 0.07	0.22 ± 0.11	0.06	14.1/16
CBAR (c fixed)	-1.23 ± 0.07	0.23 ± 0.12	0.10	14.1/16
Layter et al.[7]	-1.08 ± 0.014	0.034±0.027	0.046±0.031	17.9/18
Gormley et al.[17]	-1.17 ±0.02	0.21 ± 0.03	0.06 ± 0.04	15.3/18
Theory	a	b	c	χ^2/N
χPT [6]	-1.33	0.42	0.08	16.8/18
Kambor et al. [18]	-1.16	0.24	0.09	17.6/18
Kambor et al. (improved) [18]	-1.16	0.26	0.10	18.7/18

Table 17: Parameter for the distribution $M^2(x, y) = N(1 + ay + by^2 + cx^2)$. The χ^2/N value is given for a fit to the CBAR data of the specified functions. For the fits to the other experiments and the theory no errors in a, b and c are taken into account.

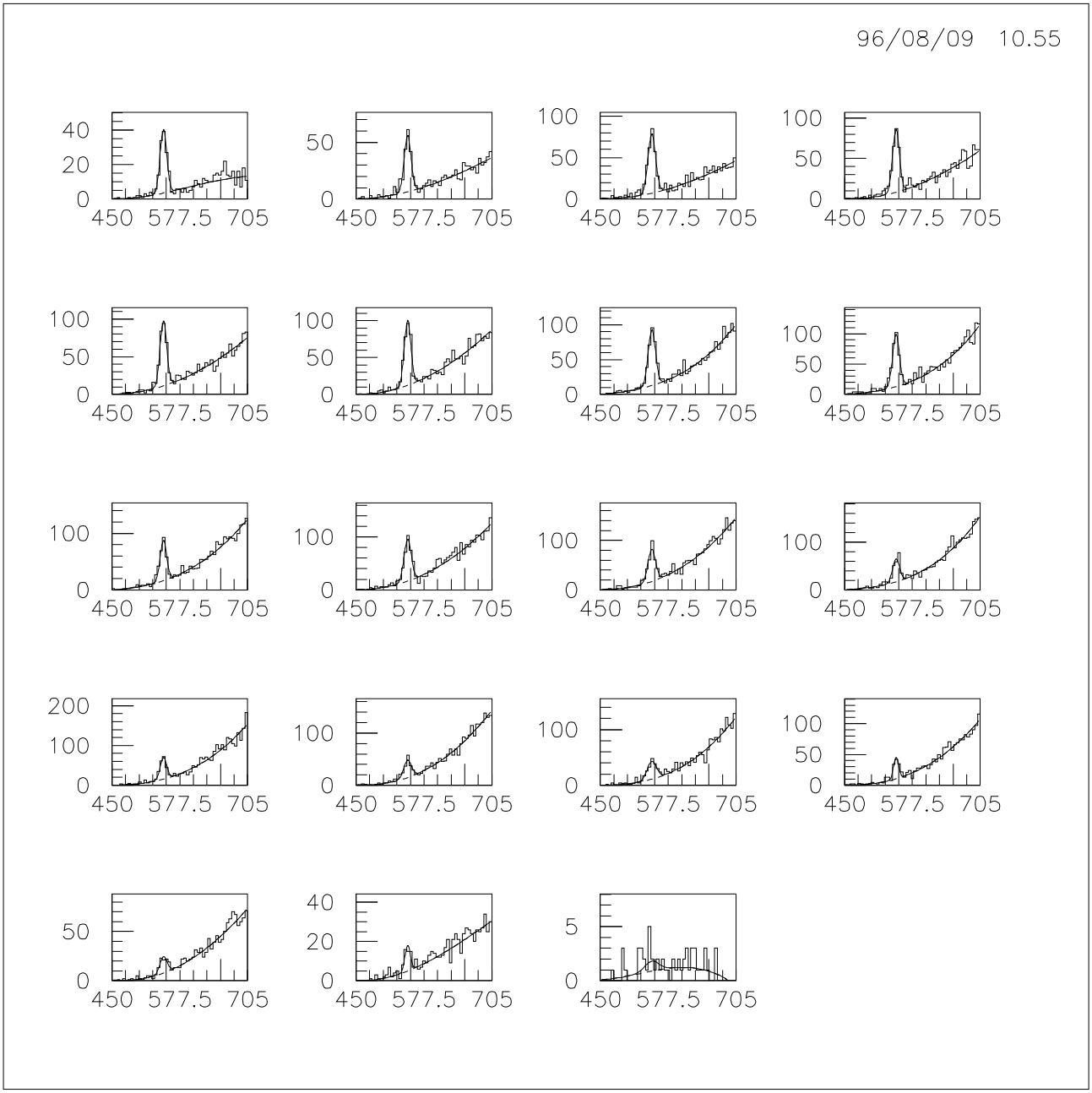

Figure 14: Fits to the invariant $m(\pi^+\pi^-\pi^0)$ distribution for the different bins of the Dalitz plot variable y. $y_1 = -1.0 - -0.9, \ldots, y_{19} = 0.8 - 0.9$.

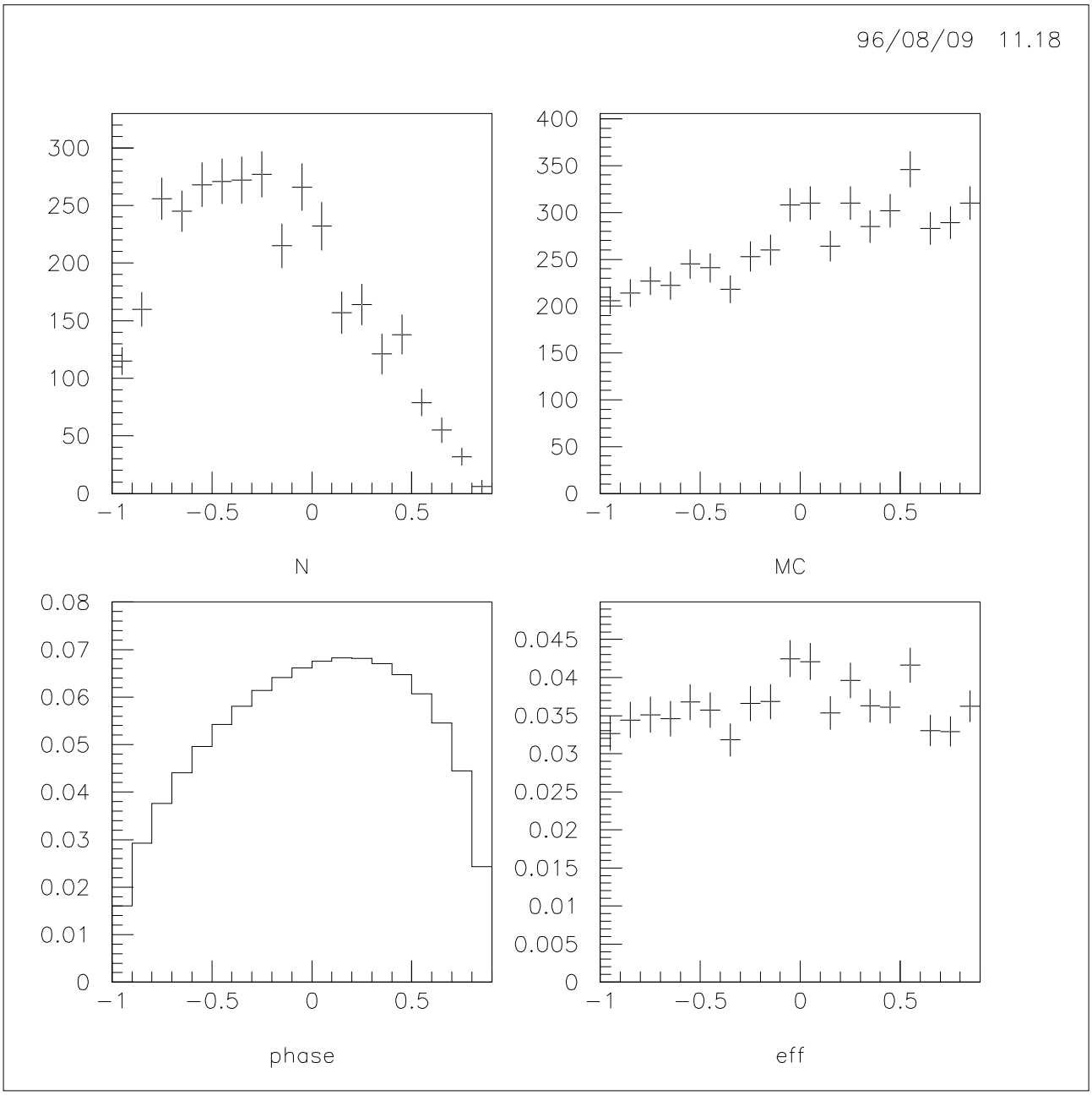

Figure 15: Distribution of the fitted number of η in data (N) and Monte Carlo (MC) versus y. Phase space distribution (phase) and efficiency (eff) versus y for the decay $\eta \to \pi^+\pi^-\pi^0$.

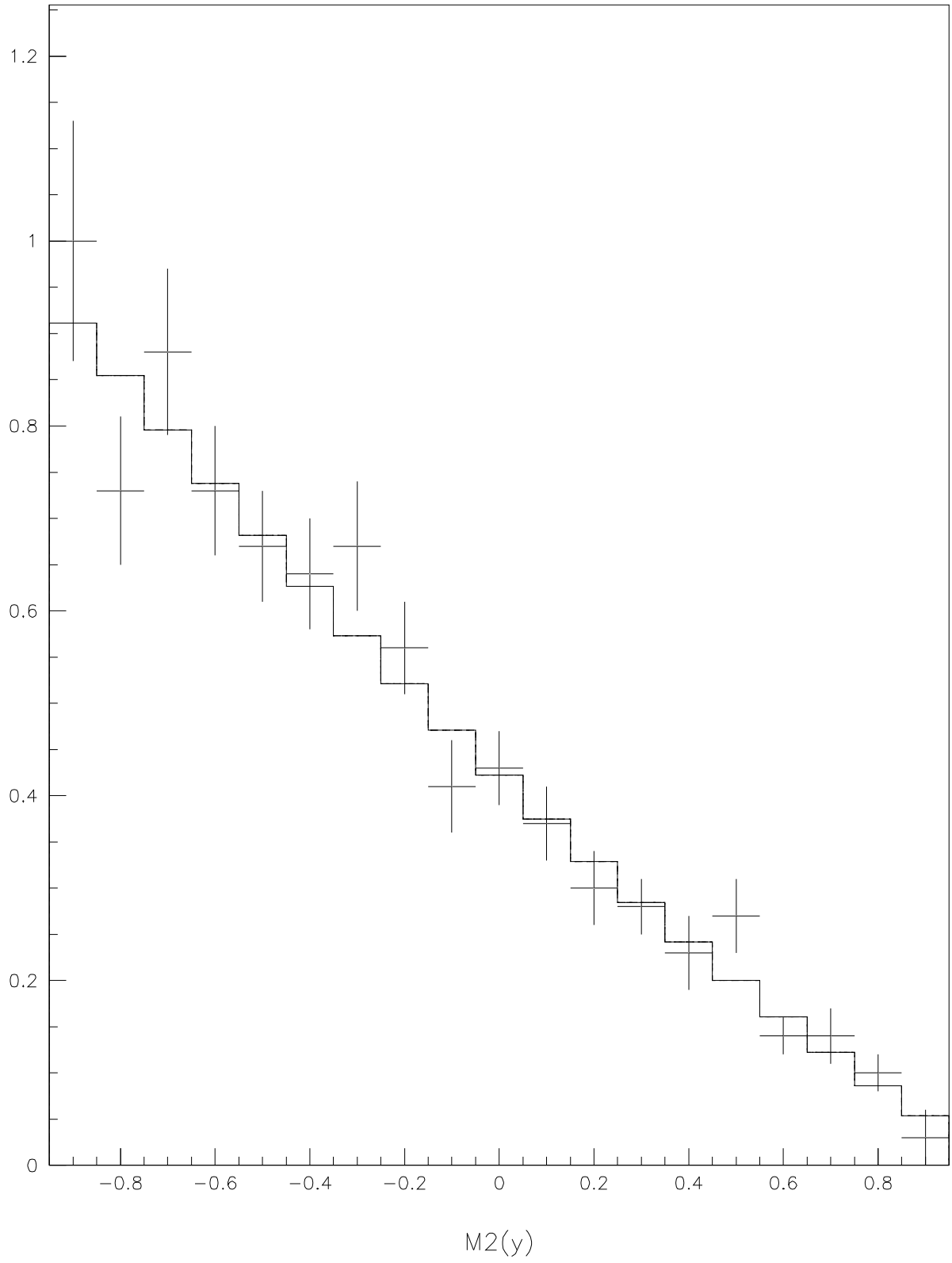

Figure 16: Phase space normalized projection of the $\eta \to \pi^+\pi^-\pi^0$ Dalitz plot on to the y-axes. Shown are the data points and a fit to our data using the function $N(1 + ay + by^2)$ (solid line).

Appendix A : Models and Relations in η/η' Decays

A1 The Chanowitz Equations

The quantities E_X and B_X introduced above are functions generally approximated by their values at the chiral point. In the form proposed by Chanowitz [1, 2], they are written :

$$\left\{ \begin{array}{ll} B_\eta(0) & = -\dfrac{\alpha_{em}}{\pi\sqrt{3}} \left[\dfrac{\cos\theta_{PS}}{f_8} - 2\sqrt{2}\ \xi \dfrac{\sin\theta_{PS}}{f_1} \right] \\ B_{\eta'}(0) & = -\dfrac{\alpha_{em}}{\pi\sqrt{3}} \left[\dfrac{\sin\theta_{PS}}{f_8} + 2\sqrt{2}\ \xi \dfrac{\cos\theta_{PS}}{f_1} \right] \end{array} \right. \qquad (A\ .\ 1\ )$$

and :

$$\left\{ \begin{array}{ll} E_\eta(0) & = -\dfrac{e}{4\pi^2\sqrt{3}} \dfrac{1}{f_\pi^2} \left[\dfrac{\cos\theta_{PS}}{f_8} - \sqrt{2} \dfrac{\sin\theta_{PS}}{f_1} \right] \\ E_{\eta'}(0) & = -\dfrac{e}{4\pi^2\sqrt{3}} \dfrac{1}{f_\pi^2} \left[\dfrac{\sin\theta_{PS}}{f_8} + \sqrt{2} \dfrac{\cos\theta_{PS}}{f_1} \right] \end{array} \right. \qquad (A\ .\ 2\ )$$

These equations connect a phase space term contribution with the pseudoscalar meson parameters : the singlet and octet coupling constants, and the mixing angle. $e = \sqrt{(}4\pi\alpha$ is the fine structure constant and $f_\pi = 93$ MeV is the pion decay constant. A consistency study of these equations shows [3] that their left–hand sides should be negative.

The parameter ξ which occurs in rels. (A.1) is connected with the underlying theory of strong interactions ; it only appears in the triangle anomaly constant which explains the two–photon decays of isoscalar pseudoscalar mesons.

If QCD holds, we have necessarily $\xi = 1$. In most realizations of integral–quark charge models $\xi = 2$. This allows for a test of QCD in its most stringent prediction.

A2 A Relation using J/ψ Decays

Using a relation of Novikov [8], Akhoury and Frère [9] have derived a useful relation :

$$\frac{\Gamma(J/\psi \to \eta'\gamma)}{\Gamma(J/\psi \to \eta\gamma)} = \left[\frac{M_{J/\psi}^2 - M_{\eta'}^2}{M_{J/\psi}^2 - M_\eta^2} \right]^3 \left[\frac{M_{\eta'}}{M_\eta} \right]^4 \left[\frac{\sqrt{2}/f_8 \cos\theta_{PS} + 1/f_1 \sin\theta_{PS}}{1/f_1 \cos\theta_{PS} - \sqrt{2}/f_8 \sin\theta_{PS}} \right]^2 \qquad (A\ .\ 3\ )$$

where the numerical factor is simply the ratio of the phase space terms in the J/ψ radiative decays to η' and η. In connection with the ξ test of QCD this relation has not to be changed if ξ is allowed to get values different of 1. This is simply connected with the fact that these processes involve a single photon.

References

[1] M. S. Chanowitz, Phys. Rev. Lett. **35**, 977 (1975).

[2] M. S. Chanowitz, Phys. Rev. Lett. **44**, 59 (1980).

[3] M. Benayoun *et al.*, Zeit. Phys. **C58**, 31 (1993).

[4] M. Benayoun *et al.*, Zeit. Phys. **C65**, 399 (1995).

[5] C. Amsler *et al.*, Phys. Lett. **B346**, 203 (1995).

[6] J. Gasser and H. Leutwyler, Nucl. Phys. **B250**, 539 (1985).

[7] J. G. Layter *et al.*, Phys. Rev. **D7**, 2565 (1973).

[8] V. A. Novikov *et al.*, Nucl. Phys. **B165**, 55 (1980).

[9] R. Akhoury and J.-M. Frère, Phys. Lett. **B220**, 258 (1989).

[10] L. M. Barkov *et al.*, Nucl. Phys. **B256**, 365 (1985).

[11] M. Bando *et al.*, Phys. Rev. Lett. **54**, 1215 (1985).

[12] H. B. O'Connel *et al.*, Phys. Lett. **B354**, 14 (1995).

[13] P. L. Chung *et al.*, Phys. Lett. **B205**, 545 (1988).

[14] G. J. Gounaris and J. J. Sakurai, Phys. Rev. Lett. **21**, 244 (1968).

[15] C. Amsler *et al.*, Phys. Lett. **B294**, 451 (1992).

[16] R. Barnett *et al.*, Phys. Rev. **D54**, 1 (1996).

[17] M. Gormley *et al.*, Phys. Rev. **D2**, 501 (1970).

[18] J. Kambor, C. Wiesendanger, and D. Wyler, Nucl. Phys. **B465**, 215 (1996).